Manuscript Details

Manuscript number	POTE_2018_1045_R1
Title	STRUCTURAL ANALYSIS OF MAGNETIC NANOCOMPOSITES BASED ON CHITOSAN
Article type	Research Paper

Abstract

This work investigates the structure and magnetic properties of chitosan based films with different contents of magnetic nanoparticles (MNPs) of around 10 nm as well as the effects of the addition of glycerol as plasticizer. Synthesized MNPs were dispersed in the chitosan film forming solution by ultrasonication and then composite films were obtained by casting. From the morphological analysis, a bimodal distribution of clusters was detected; the larger ones seem to be present mostly in the plasticized samples. Regarding the mechanical behavior of the samples, for the non-plasticized samples the outstanding increase in modulus and strength with the increasing content of MNP was explained by a strong interfacial adhesion and very good particles dispersion into the chitosan matrix. This fact was also supported by the model applyed to the strength as a function of the volume fraction of MNP. Regarding magnetic properties, all nanocomposite films evidenced systems with particles of strong dipolar interactions that lead to blocking and irreversibility temperatures close to room temperature (RT). Even though the isothermal magnetization results showed that the particles in the nanocomposite films behave as super-paramagnetic at the highest analyzed temperature (RT), Langevin model as well as FESEM and SAXS analysis supported the hypothesis that the formation of aggregates with different features dominates the magnetic response through collective behavior, mainly in the plasticized films.

Keywords	Nanocomposite films; chitosan; iron oxide nanoparticles; magnetic properties.
Manuscript category	PLASTICS (modelling, bio-based materials, biodegradation, spectroscopy, microscopy, heat and mass transport properties, foams)

Corresponding Author	Mirna Mosiewicki
Corresponding Author's Institution	Instituto de Investigaciones en Ciencia y Tecnología de Materiales (INTEMA), Facultad de Ingeniería, Universidad Nacional de Mar del Plata – CONICET
Order of Authors	Gianina A. Kloster, Diego Muraca, Oscar Moscoso Londoño, Marcelo Knobel, Norma Marcovich, Mirna Mosiewicki

Suggested reviewers	Dai Lam Tran, Victorino Franco, Aiping Zhu, Alessandro Gandini, Marcelo Villar

Submission Files Included in this PDF

File Name [File Type]

Response to reviewers.docx [Response to Reviewers]

Highlights.docx [Highlights]

Manuscript.docx [Manuscript File]

Supporting Information.docx [Supporting File]

To view all the submission files, including those not included in the PDF, click on the manuscript title on your EVISE Homepage, then click 'Download zip file'.

18th September 2018.

Prof. Mikael Hedenqvist
Editor
Polymer Testing

Ref: POTE_2018_1045
Title: STRUCTURAL ANALYSIS OF NANOCOMPOSITES WITH MAGNETIC CHARACTER BASED ON CHITOSAN (title of the original submission: SYNTHESIS AND STRUCTURAL CHARACTERIZATION OF NANOCOMPOSITES WITH MAGNETIC CHARACTER BASED ON CHITOSAN)

Authors: Gianina A. Kloster, Diego Muraca, Oscar Moscoso Londoño, Marcelo Knobel, Norma E. Marcovich and Mirna A. Mosiewicki.

Dear Prof. Mikael Hedenqvist,

We are sending to you the corrected version of our manuscript. We have carefully revised the manuscript according to the comments of the reviewers, as addressed below.

Comments from the editors and reviewers:
-**Reviewer 1**

Comments on „STRUCTURAL ANALYSIS OF NANOCOMPOSITES WITH MAGNETIC CHARACTER BASED ON CHITOSAN" (POTE_2018_1045).

The manuscript by Kloster et al. describes the preparation and characterization of several chitosan films containing various amounts of magnetic nanoparticles (magnetic iron oxides). The authors used several methods in the studies, for example X-ray diffraction, TEM, SAXS, TGA, and FE-SEM. In general, the work is fine and thorough. I do, however, have a problem with the novelty of the manuscript. Incorporation of iron oxide nanoparticles into chitosan matrices is well known in the literature. Also, the authors have published an article on the production of chitosan nanocomposite films via in situ magnetite synthesis. Therefore, the most important for this work is to compare the results with those previously reported in the literature and to show the novelty and improvements, especially why the present method of preparation is better than others.

-*We thank very much the reviewer comments about the fineness and completeness of our manuscript and we confirm that the aim of it is justly, to compare the results with those previously reported in the literature (including our own results), trying to explain the observed differences and similarities on a scientific basis. Anyhow we want to point out that although there are, in fact, a lot of papers that deal with chitosan/magnetite composites, most of the research efforts in this topic were focused to the preparation and characterization of composite particles (i.e. chitosan used as a coating onto the magnetite core) while the behavior of magnetic/chitosan composite films (i.e. a continuous chitosan matrix containing magnetite particles as filler) was scarcely studied despite the good film forming properties of the biopolymer.*

Some detailed remarks:

1. The title should be corrected. The current suggests that chitosan has magnetic character.

-According to the suggestion of the reviewer, the title was modified.

2. The language needs to be improved, for example "quitosan" is not in English.

-The reviewer was right and thus, the English of the manuscript was proofread and improved.

3. How did the authors determine the film thickness?

-It was measured with a micrometer in five random locations of the film. Just to clarify this point we added a new paragraph in the manuscript.

4. What type of sonicator was used for sample preparation? This is important, because sonication can degrade the polymer.

-As it is know, sonication is of great importance in this type of materials in order to efficiently disperse the nanoparticles in the film forming suspension. However, the reviewer is right about the fact that sonication can degrade the polymer. In order to minimize any change in the polymer conformation and/or structure, the time of sonication used was optimized to be the minimum to obtain macroscopically homogeneous dispersions. Taking into account this fact, even when we did not make any study of degradation induced by sonication, all the suspensions, including chitosan solutions without particles, were put through under the same sonication conditions in order to have the same preparation method in all the films and consequently, comparative results. In addition, the information about the sonicator used in this work was included in the "Preparation of composite films" section.

5. The effect of the MNP presence on the temperature of chitosan degradation is very interesting. However, the explanation of this effect seems unreasonable. The temperature reduction is rather too large to be assign to the changes in polymer conformation.

-We appreciate very much the comment of the reviewer. Right now we can ensure that we read all the related scientific papers we could trace in order to find any convincing explanation to this behavior. However, and although we confirmed that the presence of MNP decreases the thermal resistance of chitosan samples, we only can conclude that there are many different factors that contribute to this complex degradation process, but not quantifying their relative importance. Thus, we added new information to the original text, trying to expand the original information:

"Regarding magnetic composite films, it can be observed that the addition of MNP only slightly affects the degradation at the first and second steps. However, the temperatures related with the third step (temperature at the maximum degradation rate and the initial decomposition temperature) decrease significantly as the iron oxide content increases (Table 1). This effect was also noticed in other related works, for example, in our previous work we associated it with the changes in the conformation of the chitosan surrounding the particles in comparison with the chitosan in bulk [Kloster et al, 2015]. Soto et al (2018) also reported a decreased thermal stability, in comparison with that of the neat polymeric matrix, in their nanocomposite films based on a commercial shape memory polyurethane and different contents of magnetic iron oxides, which was associated to the increase in the thermal conductivity and thermal diffusivity of the material due to the addition of MNP. Additionally, Bertolino et al (2018) found that their nanocomposites based on chitosan and halloysite nanotubes, also prepared by casting, did not present any thermal stabilization effect due to the presence of particles. They related this fact to the adsorption of positive biopolymer on the halloysite external

surface, also with positive charge. In our case it should be noticed that chitosan - MNP suspensions were prepared in acetic acid solutions (i.e. acidic pH) and in this condition both, chitosan and Fe_3O_4 nanoparticles, are also positively charged (i.e. the isoelectric point of the MNP is around 6.85 as reported in Xu et al, 2006; Regazzoni et al, 1981 and Kloster et al, 2017. Moreover, Moeini et al (2018) indicated for chitosan based microbeads cross-linked by using sodium tripolyphosphate (TPP) that some domains in which the electrostatic repulsion prevailed could trigger a less packed structure more prone to the thermal degradation, which match exactly the present case. In this sense, these changes in the macromolecular backbone structure of the polymer would induce the weakening of the attractive intra-inter-molecular hydrogen bonds and thus, chitosan macromolecular chains would result more exposed to the random splitting of the glycosidic bonds that takes place during the thermal degradation process. Additionally, Ziegler-Borowska et al (2016) indicated that a slight decrease in the initial decomposition temperature of the magnetite-modified chitosan nanocomposite particles, in comparison with the respective chitosan derivatives (including unmodified chitosan), was observed in all cases and attributed to the presence of Fe_3O_4. They concluded that magnetite exhibited a catalytic action on the thermal degradation of chitosan and its derivatives, but did not outline any explanation for this behavior. Moreover, in a previous publication (Ziegler-Borowska et al, 2015) they emphasized that magnetite NPs enhance thermo-oxidative degradation of polymers. In brief, we believe that the decreased thermal stability of the nanocomposites, in comparison to those of the corresponding neat matrices, is due to several complex and interrelated factors.

<u>References:</u>

-G.A. Kloster, N.E. Marcovich, M.A. Mosiewicki, Composite films based on chitosan and nanomagnetite, European Polymer Journal. 66 (2015) 386–396. doi:10.1016/j.eurpolymj.2015.02.042.

-G.D. Soto, C. Meiorin, D. Actis, P. Mendoza Zélis, M.A. Mosiewicki, N.E. Marcovich, Nanocomposites with shape memory behavior based on a segmented polyurethane and magnetic nanostructures, Polymer Testing. 65 (2018) 360–368. doi:10.1016/j.polymertesting.2017.12.012.

-V. Bertolino, G. Cavallaro, G. Lazzara, S. Milioto, F. Parisi, Halloysite nanotubes sandwiched between chitosan layers: Novel bionanocomposites with multilayer structures, New Journal of Chemistry. 42 (2018) 8384–8390. doi:10.1039/c8nj01161c.

-X.Q. Xu, H. Shen, J.R. Xu, M.Q. Xie, X.J. Li, The colloidal stability and core-shell structure of magnetite nanoparticles coated with alginate, Applied Surface Science. 253 (2006) 2158–2164. doi:10.1016/j.apsusc.2006.04.015.

-A.E. Regazzoni, G.A. Urrutia, M.A. Blesa, A.J.G. Maroto, Some observations on the composition and morphology of synthetic magnetites obtained by different routes, Journal of Inorganic and Nuclear Chemistry. 43 (1981) 1489–1493. doi:10.1016/0022-1902(81)80322-3.

-G.A. Kloster, D. Muraca, M.A. Mosiewicki, N.E. Marcovich, Magnetic composite fi lms based on alginate and nano-iron oxide particles obtained by synthesis " in situ ," European Polymer Journal. 94 (2017) 43–55.

-A. Moeini, A. Cimmino, G. Dal Poggetto, M. Di Biase, A. Evidente, M. Masi, P. Lavermicocca, F. Valerio, A. Leone, G. Santagata, M. Malinconico, Effect of pH and TPP concentration on chemico-physical properties, release kinetics and antifungal activity of Chitosan-TPP-Ungeremine microbeads, Carbohydrate Polymers. 195 (2018)

631–641. doi:10.1016/j.carbpol.2018.05.005.
-M. Ziegler-Borowska, D. Chełminiak, H. Kaczmarek, A. Kaczmarek-Kędziera, Effect of side substituents on thermal stability of the modified chitosan and its nanocomposites with magnetite, Journal of Thermal Analysis and Calorimetry. 124 (2016) 1267–1280. doi:10.1007/s10973-016-5260-x.
-M. Ziegler-Borowska, D. Chełminiak, H. Kaczmarek, Thermal stability of magnetic nanoparticles coated by blends of modified chitosan and poly(quaternary ammonium) salt, Journal of Thermal Analysis and Calorimetry. 119 (2015) 499–506. doi:10.1007/s10973-014-4122-7.

6. Page 13, does the formation of MNP clusters have any advantages over homogenously dispersed magnetic particles?

-Depending on the application, the formation of clusters from individual nanoparticles could present some advantages in comparison with systems containing more homogeneously dispersed magnetic nanoparticles.

Certainly the magnetic response of the clusters is different than that of the individual particles. When the particles are close enough, the magnetic moment of each particle will be affected by those of the neighbor ones due to magnetic dipolar interactions. Thus, the magnetic moment of an agglomerate of magnetic nanoparticles will be different from the individual magnetic moment of each nanoparticle (Knobel et al, 2004). Considering that one of the possible applications for these films is their use in water remediation (i.e. removal of ions from water), the possibility of heating by application of an external magnetic field can be a useful characteristic to activate the adsorption/desorption character of these materials when immersed in the fluid, just to mention one specific example.
However, results regarding the most efficient nanoparticles configuration (agglomerated or totally dispersed) are still controversial. While it is expected that fully dispersed nanoparticles should be the best nanoparticle configuration, several reports show that inter-particle dipole interactions in clusters can contribute positively to magnetic hyperthermia or magnetic heating properties. For example, Fu et al (2018) recently indicated that "dipole interactions are inclined to improve the hyperthermia heating only when the clusters are small enough to induce an enhancement in clusters' shape anisotropy. Once the clusters are losing their shape anisotropy, dipole interactions will change to impair the heating. When the clusters are totally isotropic in shape, it is hard for them to provide a heating better than non-interacting particles do, even though the heating efficiency could rebound by somewhat at a particular size."
Anyhow, in order to confirm that the clusters of nanoparticles are improving the efficiency of the composite for the specific case reported here, we need to compare its behavior with that of a similar system made from perfectly dispersed nanoparticles, which is far from the scope of this work.

Alternatively, regarding mechanical properties of composites, the change of the properties (i.e. modulus, resistance, elongation at break) with respect to those of the neat matrix is expected to be higher, for the same concentration of filler, if the particles are homogenously dispersed. Moreover, in any property that needs a strong

interaction particle-matrix, homogenously dispersed particles are preferable to clusters, due to the favorable ratio area/volume of the former configuration.

On the other hand, the method of preparation not only changes the dispersion and size of the particles and/or clusters into the matrix. Different methods of synthesis lead to different degrees of interaction of the particles with the matrix and the amount of plasticizer that can be retained into the film (see answer to reviewer 2). The synthesis of magnetic particles and posterior incorporation into the chitosan solution seems to lead to a weaker interaction between matrix and particles/clusters than the "in situ" synthesis and in this way; the magnetic entities are freer to react in the presence of an external magnetic field. In addition, this last method allows a better control of the amount of plasticizer required in the films that can significantly affect some specific properties (for example, mechanical ones) in comparison with that of the nanocomposite films prepared by the "in situ" method.

References:

-M. Knobel, L.M. Socolovsky, J.M. Vargas, Propiedades magnéticas y de transporte de sistemas nanocristalinos : conceptos básicos y aplicaciones a sistemas reales, Revista Mexicana de Física. 50 (2004) 8–28.

-R. Fu, Y. Yan, C. Roberts, Z. Liu, Y. Chen, The role of dipole interactions in hyperthermia heating colloidal clusters of densely-packed superparamagnetic nanoparticles, Scientific Reports. 8 (2018) 1–10. doi:10.1038/s41598-018-23225-5.

7. Page 15, the authors wrote "The increase of modulus is related with the high rigidity of the MNP in comparison with that of the polymeric matrix and can be expected if the particles are homogeneously distributed and no pores or bubbles are generated during drying of the composite". However, the MNP particles are not homogeneously distributed in the chitosan matrix, as shown in Figure 3.

-Even when the particles can group forming clusters of obviously higher sizes than that of the individual entities, these agglomerates can also be homogeneously distributed into the matrix and contribute to increase the modulus of the composite. Anyhow, we modified the corresponding paragraph in order to clarify this point.

8. The conclusion, "A simple procedure" is not true. The presented procedure is more complicated compared to the "in situ" method, since it requires isolation of MNP particles and resuspension in the chitosan solution.

-We clearly understood the point of view of the reviewer and therefore we want to make some clarifications. The "in situ" method seems to be simpler than that used in this work at least in the first step of preparation because the particles are not synthesized prior to their incorporation into the matrix. However, the final steps of the "in situ" method are not so simple. In fact, the "in situ" method requires first the film formation (drying in a convective oven), then the immersion of the film into the alkali solution to induce the particle formation, then successive washes until neutral pH. These steps make more complex the procedure and even part of the plasticizer can be lost in the successive washings, cracking/void formation in the film can be induced due to manipulation or partial solubilization/disintegration of the polymeric matrix, etc. However, we agree with the reviewer that the phrase "A simple procedure" is not the more representative for this system and thus, we modified the "conclusions" section according with this idea.

-**Reviewer** **2**

- In the description of FE-SEM it should be indicated that cryofracture surface of films were analyzed.

- This information was included in this revised version of the manuscript.

A comment or intepretation of the effect of glycerol on the initial temperature of degradation and the temperature of maximum degradation rate for the 3rd step mus be included.

- We appreciate this observation. A new paragraph was added in the section corresponding to thermal degradation analysis to take into account the comment of the reviewer, as follows:

Table 1 presents the temperature at the maximum degradation rate and the initial decomposition temperature of the last degradation step. It is clear that the plasticizer produces a movement of the third step to higher temperatures. Higher thermal stability with the presence of glycerol in films of chitosan was also reported in the works of Debandi and co-workers (2016) and Fundo et al (2015). In the last case, authors indicated that plasticizer addition increased the melting enthalpy, i.e., increases the samples crystallinity, and attributed this effect to glycerol interaction with chitosan chains indicating that the H-bonds stabilize chitosan crystals. They also noticed that the main peak shifted to higher melting temperatures when increasing plasticizer concentration, which correlated well with other published results [Rivero et al, 2010] and may be also related with an increase of the strength of the H-bonds stabilizing chitosan crystals in the presence of plasticizer, as indicated by [Okuyama et al, 1997]. Thus, although part of the glycerol is lost in the first stage of degradation, as was mentioned above, a high percentage remain retained in the polymer structure because of these strong intermolecular interactions developed with chitosan. As a consequence, plasticized samples are not only more crystalline than unplasticized films, but also contain more stable crystals that start to degrade at higher temperature. Moreover, due to the different initial structures of plasticized and non plasticized films, there should be diffusive changes in the volatile products and pyrolysis wastes generated in the second step of degradation that also could affect the degradation pattern of the last step.

References:

-M. V. Debandi, C. Bernal, N.J. Francois, Development of biodegradable films based on chitosan/glycerol blends suitable for biomedical applications, Journal of Tissue Science & Engineering. 07 (2016). doi:10.4172/2157-7552.1000187.
-J.F. Fundo, A.C. Galvis-Sanchez, I. Delgadillo, C.L.M. Silva, M.A.C. Quintas, The effect of polymer/ plasticiser ratio in film forming solutions on the properties of chitosan films, Food Biophysics. 10 (2015) 324–333. doi:10.1007/s11483-015-9394-3.
-S. Rivero, M.A. García, A. Pinotti, Correlations between structural, barrier, thermal and mechanical properties of plasticized gelatin films, Innovative Food Science and Emerging Technologies. 11 (2010) 369–375. doi:10.1016/j.ifset.2009.07.005.
-K. Okuyama, K. Noguchi, T. Miyazawa, T. Yui, K. Ogawa, Molecular and crystal structure of hydrated chitosan, Macromolecules. 30 (1997) 5849–5855. doi:10.1021/ma970509n.

Since glycerol content was constant for all the plaxticized samples authors must revised the phrase: "The ultimate deformation does not present a clear trend, neither with respect to magnetite concentration, nor with respect to glycerol content"

-All the plasticized samples present the same content of glycerol with respect to the chitosan mass; however, the phrase is related with the insignificant variation in the ultimate deformation comparing plasticized samples with unplasticized ones.

Anyhow and to avoid misunderstandings, a phrase was added to the original paragraph, as follows:

" nor with respect to glycerol content (i.e. comparing S samples with SG samples at fixed magnetite concentration)."

Please, let us know if further explanations or corrections are needed.

Sincerely yours,

Dr Mirna A. Mosiewicki
mirna@fi.mdp.edu.ar

STRUCTURAL ANALYSIS OF MAGNETIC NANOCOMPOSITES BASED ON CHITOSAN

Gianina A. Kloster[a], Diego Muraca[b], Oscar Moscoso Londoño[b,c], Marcelo Knobel[b], Norma E. Marcovich[a] and Mirna A. Mosiewicki[a*]

Highlights

- Magnetic nanocomposite films based on chitosan and magnetic iron oxides were obtained.
- For the non-plasticized films, iron oxide nanoparticles have a mechanical reinforce effect.
- Strong interfacial adhesion between matrix and particles support the analyzed results.
- Magnetic and SAXS analysis evidence the formation of aggregates.
- Bimodal cluster size distribution was detected.

STRUCTURAL ANALYSIS OF MAGNETIC NANOCOMPOSITES BASED ON CHITOSAN

Gianina A. Kloster[a], Diego Muraca[b], Oscar Moscoso Londoño[b,c], Marcelo Knobel[b], Norma E. Marcovich[a] and Mirna A. Mosiewicki[a*]

[a]Instituto de Investigaciones en Ciencia y Tecnología de Materiales (INTEMA), Facultad de Ingeniería, Universidad Nacional de Mar del Plata – CONICET, Mar del Plata, Argentina.

[b]Instituto de Física Gleb Wataghin (IFGW), Universidade Estadual de Campinas – UNICAMP, Campinas, São Paulo, Brazil.

[c]Universidad Autónoma de Manizales, Facultad de Ingeniería, Antigua Estación del Ferrocarril, Manizales, Colombia.

*corresponding author: mirna@fi.mdp.edu.ar

Abstract

This work investigates the structure and magnetic properties of chitosan based films with different contents of magnetic nanoparticles (MNPs) of around 10 nm as well as the effects of the addition of glycerol as plasticizer. Synthesized MNPs were dispersed in the chitosan film forming solution by ultrasonication and then composite films were obtained by casting. From the morphological analysis, a bimodal distribution of clusters was detected; the larger ones seem to be present mostly in the plasticized samples. Regarding the mechanical behavior of the samples, for the non-plasticized samples the outstanding increase in modulus and strength with the increasing content of MNP was explained by a strong interfacial adhesion and very good particles dispersion into the chitosan matrix. This

fact was also supported by the model applyed to the strength as a function of the volume fraction of MNP.

Regarding magnetic properties, all nanocomposite films evidenced systems with particles of strong dipolar interactions that lead to blocking and irreversibility temperatures close to room temperature (RT). Even though the isothermal magnetization results showed that the particles in the nanocomposite films behave as super-paramagnetic at the highest analyzed temperature (RT), Langevin model as well as FESEM and SAXS analysis supported the hypothesis that the formation of aggregates with different features dominates the magnetic response through collective behavior, mainly in the plasticized films.

Keywords

Nanocomposite films

Chitosan

Iron oxide nanoparticles

Magnetic properties

1 INTRODUCTION

The study and use of nanocomposites based on biopolymers with a magnetic disperse phase is an important area of research in constant growth due to potential applications, including uses in biomedicine, biotechnology and wastewater treatment [1,2], for example. The choice of a polymer with chelating properties such as chitosan has shown very promising results in the treatment of contaminated water with heavy metal ions, herbicides and dyes [3–5]. Chitosan is a biodegradable polymer extracted from the deacetylation of the chitin, major component of crustacean's shells and fungal biomass.

This cationic polysaccharide, composed by β-(1,4)-2-amino-2-deoxy-D-glucopyranose units and small quantity of N-acetyl-D-glucosamine residues [6,7], displays interesting properties including biocompatibility, non-toxicity, good film forming ability, antibacterial and antifungal activity [8]. It contains several reactive groups that interact with metal ions through various mechanisms depending on the involved ion, the pH, and solution composition [9], acting as an excellent adsorbent agent.

The incorporation of iron oxide nanoparticles (NPs) as a disperse phase allows obtaining a nanocomposite that could provide interesting properties. For example, these nanocomposites could be easily removed from water with the help of an external magnet [10], while remaining environmental friendly due to the low toxicity and biocompatible characteristics of the iron oxides [11]. The magnetic properties of the composites will be determined principally by the nanoparticle magnetic properties and their interactions. When the size of the iron oxide NPs is below a critical size (<15 nm [12]), they could exhibit superparamagnetic behavior and thus, even embedded in a polymeric matrix, the magnetic moment of each NP will follow the direction of the applied magnetic field allowing to move or attract the nanocomposite with an external magnetic field. In this line, Zhuang et al. [13] have synthesized Fe_3O_4−SiO_2−SrHAp microspheres for the immobilization of Pb (II), which were simply collected from water by magnetic separation.

The interaction between chitosan and iron oxides NPs is explained through complex mechanisms of electrostatic forces and interactions occurring between polar groups [14–18]. Different methods of synthesis have been applied to obtain chitosan/iron oxide nanocomposites. For instance, Bezdorozhev et al. [19] have reported the synthesis of magnetite-chitosan nanostructures by the chemical precipitation of magnetite NPs in the

presence of chitosan. In that work, the authors vary some synthesis parameters to study their influence on the nanoparticle morphology. Singh and co-workers [20] fabricated nanocomposite films based on hydrothermally prepared hematite (α-Fe_2O_3) NPs and chitosan using glycolic acid as organic surfactant. According to the authors, the obtained NPs had an irregular spheroidal shape with a mean diameter of 110 nm. The coating of magnetic particles has been extensively used to control or tune their agglomeration and to assist the size control of particles due to cross-linking among NPs with chitosan, fact extremely important in order to achieve the desired physical or chemical behavior. A good example of this is the work published by Bhatt et al. [21], where iron oxide NPs were synthesized separately (via the hydrothermal process) and then dispersed into the chitosan solution by ultrasonication, resulting in materials with new electrical and magnetic properties.

However, and depending on the application envisaged for the magnetic nanocomposite, the formation of clusters from individual nanoparticles could present some advantages in comparison with systems containing more homogeneously dispersed magnetic nanoparticles. The magnetic response of the clusters is different than that of the individual particles. When the particles are close enough, the magnetic moment of each particle will be affected by those of the neighbor ones due to magnetic dipolar interactions. Thus, the magnetic moment of an agglomerate of magnetic nanoparticles will be different from the individual magnetic moment of each nanoparticle [22]. However, results regarding the most efficient nanoparticles configuration (agglomerated or totally dispersed) are still controversial. While it is expected that fully dispersed nanoparticles should be the best nanoparticle configuration, several reports show that inter-particle

dipole interactions in clusters can contribute positively to magnetic hyperthermia or magnetic heating properties [23].

On the other hand, the method of preparation not only changes the dispersion and size of the particles and/or clusters into the matrix. Different methods of synthesis lead to different degrees of interaction of the particles with the matrix and the amount of plasticizer that can be retained into the film. The synthesis of magnetic particles and posterior incorporation into the chitosan solution could lead to a weaker interaction between matrix and particles/clusters than the "in situ" synthesis [24] and in this way; the magnetic entities would be freer to react in the presence of an external magnetic field. In addition, this last method allows a better control of the amount of plasticizer required in the films that can significantly affect some specific properties (for example, mechanical properties) in comparison with that of the nanocomposite films prepared by the “in situ” method.

In a previous work, we reported the obtaining of chitosan/MNP nanocomposite films via “in situ” synthesis of magnetite [25]; both mechanical and magnetic properties, were discussed and explained in terms of the matrix composition and nanoparticle concentration. In this work, magnetic iron oxides NPs were incorporated to a chitosan solution and dispersed by ultrasonication to obtain magnetic nanocomposite films. NPs were obtained by a simple iron oxide alkaline precipitation method, followed by washings and solvent elimination via lyophilization. The effects of the glycerol (plasticizer) and magnetic nanoparticles concentration on the physical, morphological, mechanical and magnetic properties of the films is presented and discussed. Besides, the information about these nanostructured materials was complemented by SAXS analysis by means of fitting experimental results with appropriate models.

2 EXPERIMENTAL PROCEDURES

2.1 Materials

Chitosan in powder form (degree of deacetylation 98%, Mv = 1.61×10^5 g/mol) was supplied by Parafarm. Glycerol (G), purchased from DEM Mar del Plata, was used as plasticizer. Ferric chloride hexahydrate ($FeCl_3.6H_2O$), ferrous sulphate heptahydrate ($FeSO_4.7H_2O$) and ammonium hydroxide (25% NH_3) were obtained from Aldrich. All the samples were prepared using commercially available reagents.

2.2 Methods

2.2.1 Synthesis of magnetic iron oxides nanoparticles

The iron oxide NPs were obtained by an alkaline co-precipitation method adapted from that developed by Massart and Cabuil [26]. In brief, 4.8 g of $FeSO_4.7H_20$ and 9.32 g of $FeCl_3.6H_2O$ (molar ratio Fe^{+2}:Fe^{+3}=1:2) were dissolved in approximately 40 mL of distilled water. Once the solution was perfectly homogenized, 15 mL of NH_4OH was added drop by drop in order to avoid or minimize the MNPs aggregation. The suspension was stirred for 15 minutes, allowing the complete precipitation of MNPs. After this time and with the help of a magnet placed out of the flask, several washes with distilled water were made until neutral pH. Then, the wet particles were placed into a Petri plate and lyophilized to eliminate the water. Finally, the obtained powder was kept into a dark colored glass container.

2.2.2 Preparation of composite films

Chitosan solution (2 % w/v) was prepared by dissolving chitosan powder in aqueous acetic acid solution (1% v/v) by magnetic stirring at room temperature. Glycerol, in a

weight ratio glycerol/chitosan equal 0.3, was also added to the solution when applicable. Selected amounts of MNPs were incorporated to the polymer solution to prepare nanocomposite films. Film forming suspensions were obtained by manually mixing MNPs with chitosan (or chitosan/glycerol) solution, followed by ultrasonication for 2 hours (Elmasonic P60H sonicator with a frecuency of 37 kHz and a power of 150 W). As it is know that ultrasonication can cause some degradation of the bio polymer, neat chitosan and chitosan/glycerol solutions, used to prepare control films (0% MNPs) were also sonicated. Then, the suspensions were poured into Petri dishes (diameter = 14 cm) and dried in a convective oven at 35°C for 24 hours (solvent casting). The actual MNP content of the films was determined by thermogravimetric analysis, as indicated in the following sections.

The obtained films, with thickness in the range of 200-300 μm, were kept in a closed container containing dried silica gel at room temperature (23 ± 2°C) until testing. Non-plasticized film samples were labeled as S0, S1, S2, S3, S4, S5, while a "G" was added at the end of the acronym for plasticized samples (i.e. S0G, S1G, S2G, S3G, S4G and S5G).

2.2.3 Characterization of MNPs and composite films

Film thickness: The thickness of the films was measured with a 0–25 mm manual micrometer with an accuracy of ± 0.01 mm at least at five random locations for each film. The reported values are the average of those individual measurements.

X-ray diffraction (DRX): The crystal structure of the MNPs was investigated using CuKα radiation (λ=1.5418 A) in a PANalytical X'Pert Pro diffractometer operated at 40 kV, 300 mA and 0.6 °C/min.

Transmission Electron Microscopy (TEM): TEM analysis of the MNPs was performed on a TEM-FEG (JEM 2100F) field-emission gun transmission electron microscope (voltage: 200 kV). The images were acquired using a Gatan, Orius SC600/831 camera at different resolutions. The particles were dispersed in Milli-Q water and sonicated during 15 minutes. The samples for microscopy observation were prepared by drying a drop of this suspension during 24 hours at room temperature on a Ted Pella ultrathin cooper film on a holey carbon. The obtained images were analyzed using ImageJ free software.

***Small-angle X-ray Scattering (SAXS)*:** SAXS experiments were performed on SAXS1 beamline at the Brazilian Synchrotron Light Laboratory (LNLS), Centro Nacional de Pesquisa em Energia e Materiais (CNPEM), Campinas, Brazil. The measurements were carried out at room temperature. The scattering intensity was recorded as function of momentum transfer vector q ($q = 4\pi \sin\theta/\lambda$), in a range from 0.1 to 5.0 nm^{-1}, being θ the scattering angle and λ the wavelength = 1.822 Å.

Thermogravimetric analysis (TGA): Thermogravimetric tests of the films were performed in a TGA-40 Shimadzu Thermogravimetric Analyzer at a heating rate of 10 °C/min under air atmosphere (35 mL/min) from room temperature to 900°C. Samples tested were previously dried in a vacuum oven during 2 hours at 60°C followed by 22 hours at 40°C, to remove traces of water absorbed during storage.

Field Emission Scanning Electron Microscopy (FE-SEM): The cryofractured surface (thickness) of the films were analyzed with a Carl Zeiss Supra 40 Gemini, Field Emission Scanning Electron Microscope (FE-SEM) equipped with an energy dispersive X-ray spectroscopy (EDS) attachment for elemental analysis.

Tensile properties: Tensile tests were performed at room temperature (23 ± 2º C) using an Instron Universal Testing Machine model 8501. The specimens were cut into strips of 5 x

25 mm. Five specimens from each film were tested from a minimum of three films per sample. Crosshead speed was set at 10 mm/min. The ultimate strength (σ_u), elongation at break (ε_b) and elastic modulus (E) were calculated as described in ASTM D638-94b (ASTM, 1994). Prior to running mechanical tests, films were conditioned for 72 hours at 65 ± 5% relative humidity at room temperature.

Magnetic characterization: The magnetic properties of the composite film were obtained using a commercial SQUID magnetometer (Quantum Design, MPMS XL). Both isothermal magnetization curves (*M vs. H*) as well as the temperature dependence of magnetization (*M vs. T*) were obtained. The *M vs. H* curves were recorded at 2 and 300 K in a magnetic field range of ± 1T. The M vs. T curves were recorded under the zero-field-cooling and field-cooling (ZFC/FC) protocols with a static magnetic field of 50 Oe. Samples used for these tests were previously conditioned in a closed container with silica gel until they reached their equilibrium moisture content (about 5–7 wt.%).

3 RESULTS AND DISCUSSION

3.1. Structural studies of the magnetic particles

Figure 1 shows representative transmission electron micrographs of the synthesized iron oxide NPs; the inset of Figure 1(a) shows the size distribution obtained by counting more than one hundred particles. From the analysis of the histogram, an average particle diameter of 9.5 ± 2 nm with a narrow size distribution was calculated (full line represents the best fit according to a lognormal size distribution).

Figure 1(a-b) reveals a moderate agglomeration of the particles, as can be expected for a set of magnetic NPs without surface treatments/surfactant [27]. It is also noticed that not all the particles have a spherical shape, some of them presenting shape irregularities.

Figure 1(c) shows a HR-TEM image of a selected nanoparticle. Fast Fourier Transform (FFT) was used to estimate the Bragg plane distances on the HR-TEM image allowing to identify the (113) and (044) crystallographic planes corresponding to the magnetite (Fe_3O_4) and/or maghemite (Fe_2O_3) spinel-inverse [28].

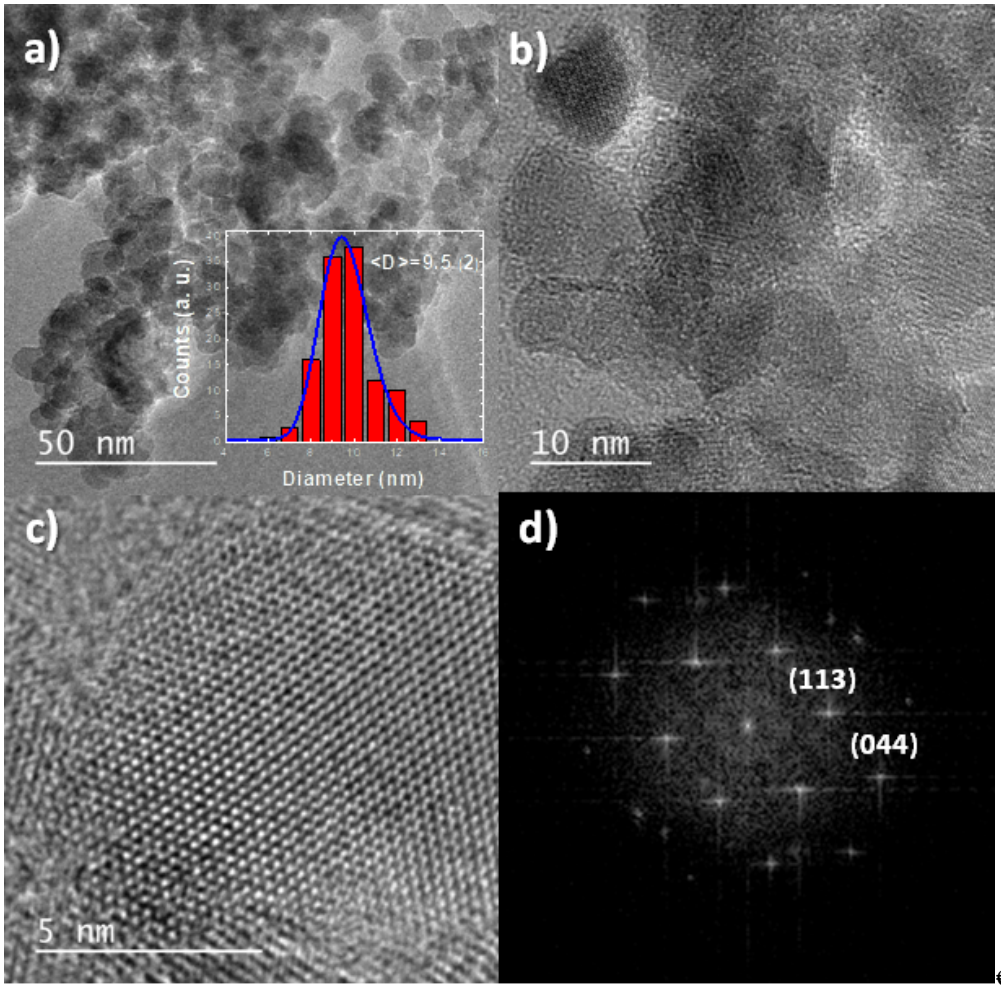

Figure 1.(a)–(b) Transmission electron microscopy at different magnifications (right corner inset of figure 1a), size distribution of these MNPs), (c) HR-TEM of selected MNP, (d) FFT of the HR-TEM on figure (c).

X-ray diffraction pattern of the synthesized particles was also analyzed (Figure S1, supplementary information). The positions and relative intensities of the diffraction peaks agree with those of a pure face-centered cubic (fcc) spinel-inverse iron oxide phase corresponding to the standard crystal of magnetite and/or maghemite [29–31]. The crystal size (D) was determined using Scherrer's equation [32–34], from which a value of D = 9.5 nm was obtained.

Despite that "crystallite size" is not necessarily synonymous of "particle size", this method gives an estimation of the diameter of the magnetic particles [27]. Notice that the obtained value is close to those determined from TEM images.

Small-angle X-ray scattering (SAXS) technique was used to analyze the morphological features of magnetic NPs before they are loaded into the chitosan matrices. Figure S2a in supplementary information presents the SAXS scattering patterns obtained from the synthesized NPs. According to the range of q parameter selected for the measurement, the NPs that could be characterized have sizes ranging between π/q_{max}=1 nm to π/q_{min} = 30 nm. From linear Guinier law at low q region (Figure S2b, supplementary information) the radius of gyration, Rg, was calculated as 6 nm [35,36].

Then, if the NPs are mostly spherical, an average diameter, Dg, of 15.4 nm was estimated indicating that possibly small aggregation of primary particles occurs when they are in a colloidal suspension. The scattering intensity in the Porod region presents a slope close to -4, which corresponds to individual particles with smooth surfaces [36,37].

3.2. Characterization of the nanocomposites films

Thermogravimetric measurements were carried out in air atmosphere in order to determine the content of MNPs effectively incorporated into the films and to study the thermal degradation of the nanocomposites. From the residual mass left at 800°C, the iron oxide content was obtained considering that the residual char corresponds to chitosan (or chitosan + glycerol) and ferric oxide, since oxidation process of magnetite into ferric oxide due to heating occurs in the range of 130-330°C, as was reported elsewhere [38,39]. The residual mass, corresponding to the matrix, was subtracted proportionally from the residual char of the composite samples and the difference was converted to magnetite mass. These calculations are listed in Table 1, as actual magnetite content. It should be mentioned that during the preparation process not all the MNP could be successfully loaded in the film forming solutions (i.e. forming a stable colloidal suspension), thus part of the magnetic solute remained at the bottom of the flask where the suspension was prepared, not being transferred to the Petri dish (mold).

Figure 2 presents the TGA curves for selected composite films prepared from neat and plasticized chitosan (S0, S3, S5, S0G, S3G, S5G). Both matrices (films without MNP) exhibit three main stages of weight loss. The first one is attributed to loss of absorbed water due to the hydrophilic character of the chitosan and, in the case of the plasticized sample, also to the loss of the free glycerol. For this reason, the loss of weight of the plasticized samples at relatively low temperature is larger than the corresponding to neat chitosan films. The second step of weight loss, with maximum degradation rate at around 270°C corresponds to the chemical degradation and deacetylation of chitosan [40]. The last step observed between ~480 and 630°C corresponds to the oxidative degradation of the carbonaceous residue, which is formed during the second step [16].

Table 1 presents the temperature at the maximum degradation rate and the initial decomposition temperature of the last degradation step. It is clear that the plasticizer produces a movement of the third step to higher temperatures. Higher thermal stability with the presence of glycerol in films of chitosan was also reported in the works of Debandi and co-workers (2016) [41] and Fundo et al (2015) [42]. In the last case, authors reported that plasticizer addition increased the melting enthalpy, i.e., increases the samples crystallinity, and attributed this effect to glycerol interaction with chitosan chains indicating that the H-bonds stabilize chitosan crystals. They also noticed that the main peak shifted to higher melting temperatures when increasing plasticizer concentration, which correlated well with other published results [43] and may be also related with an increase of the strength of the H-bonds stabilizing chitosan crystals in the presence of plasticizer, as indicated by Okuyama et al (1997) [44]. Thus, although part of the glycerol is lost in the first stage of degradation, as was mentioned above, a high percentage remain retained in the polymer structure because of these strong intermolecular interactions developed with chitosan. As a consequence, plasticized samples are not only more crystalline than unplasticized films, but also contain more stable crystals that start to degrade at higher temperature. Moreover, due to the different initial structures of plasticized and non plasticized films, there should be diffusive changes in the volatile products and pyrolysis wastes generated in the second step of degradation that also could affect the degradation pattern of the last step.

Regarding magnetic composite films, it can be observed that the addition of MNP only slightly affects the degradation at the first and second steps. However, the temperatures related with the third step (temperature at the maximum degradation rate and the initial decomposition temperature) decrease significantly as the iron oxide content increases (Table 1). This effect was also noticed in other related works, for example, in our previous

work we associated it with the changes in the conformation of the chitosan surrounding the particles in comparison with the chitosan in bulk [25]. Soto et al (2018) [45] also reported a decreased thermal stability, in comparison with that of the neat polymeric matrix, in their nanocomposite films based on a commercial shape memory polyurethane and different contents of magnetic iron oxides, which was associated to the increase in the thermal conductivity and thermal diffusivity of the material due to the addition of MNP. Additionally, Bertolino et al (2018) [46] found that their nanocomposites based on chitosan and halloysite nanotubes, also prepared by casting, did not present any thermal stabilization effect due to the presence of particles. They related this fact to the adsorption of positive biopolymer on the halloysite external surface, also with positive charge. In our case it should be noticed that chitosan - MNP suspensions were prepared in acetic acid solutions (i.e. acidic pH) and in this condition both, chitosan and Fe_3O_4 nanoparticles, are also positively charged (i.e. the isoelectric point of the MNP is around 6.85 as reported in Xu et al (2006) [47], Regazzoni et al (1981) [14] and Kloster et al (2017) [48]). Moreover, Moeini et al (2018) [49] indicated for chitosan based microbeads cross-linked by using sodium tripolyphosphate (TPP) that some domains in which the electrostatic repulsion prevailed could trigger a less packed structure more prone to the thermal degradation, which match exactly the present case. In this sense, these changes in the macromolecular backbone structure of the polymer would induce the weakening of the attractive intra-inter-molecular hydrogen bonds and thus, chitosan macromolecular chains would result more exposed to the random splitting of the glycosidic bonds that takes place during the thermal degradation process. Additionally, Ziegler-Borowska et al (2016) [50]indicated that a slight decrease in the initial decomposition temperature of the magnetite-modified chitosan nanocomposite particles, in comparison with the respective chitosan derivatives (including

unmodified chitosan), was observed in all cases and attributed to the presence of Fe_3O_4. They concluded that magnetite exhibited a catalytic action on the thermal degradation of chitosan and its derivatives, but did not outline any explanation for this behavior. Moreover, in a previous publication (Ziegler-Borowska et al, 2015) [51] they emphasized that magnetite NPs enhances thermo-oxidative degradation of polymers. In brief, we believe that the decreased thermal stability of the nanocomposites, in comparison to those of the corresponding neat matrices, is due to several complex and interrelated factors.

Table 1. Actual content of MNP of the films, initial temperature (Ti) and temperature at maximum degradation rate (Tm) of the 3rd thermal degradation step. All data were obtained from TGA analysis in air atmosphere.

Sample	MNPs actual content (wt.%)	Ti (3rd step) (°C)	Tm (3rd step) (°C)
S0	0.00	532.0 ± 16.9	574.0 ± 22.6
S1	1.2 ± 0.2	481.5 ± 17.7	510.0 ± 14.1
S2	2.2 ± 0.3	467.5 ± 2.1	489.0 ± 1.4
S3	3.0 ± 0.5	437.5 ± 2.1	459.0 ± 1.4
S4	3.7 ± 0.2	409.7 ± 8.0	436.3 ± 14.6
S5	5.8 ± 0.4	398.0 ± 7.2	416.3 ± 4.0
S0G	0.00	552.0 ± 22.6	589.5 ± 19.0
S1G	1.3 ± 0.0	509.0 ± 5.6	531.0 ± 2.8
S2G	1.6 ± 0.3	489.0 ± 7.1	510.0 ± 18.3
S3G	3.0 ± 0.4	517.5 ± 0.7	528.0 ± 8.4

S4G	3.6 ± 0.4	452.5 ± 3.5	469.0 ±11.3
S5G	4.7 ± 0.3	408.0 ± 8.4	430.5 ± 0.7

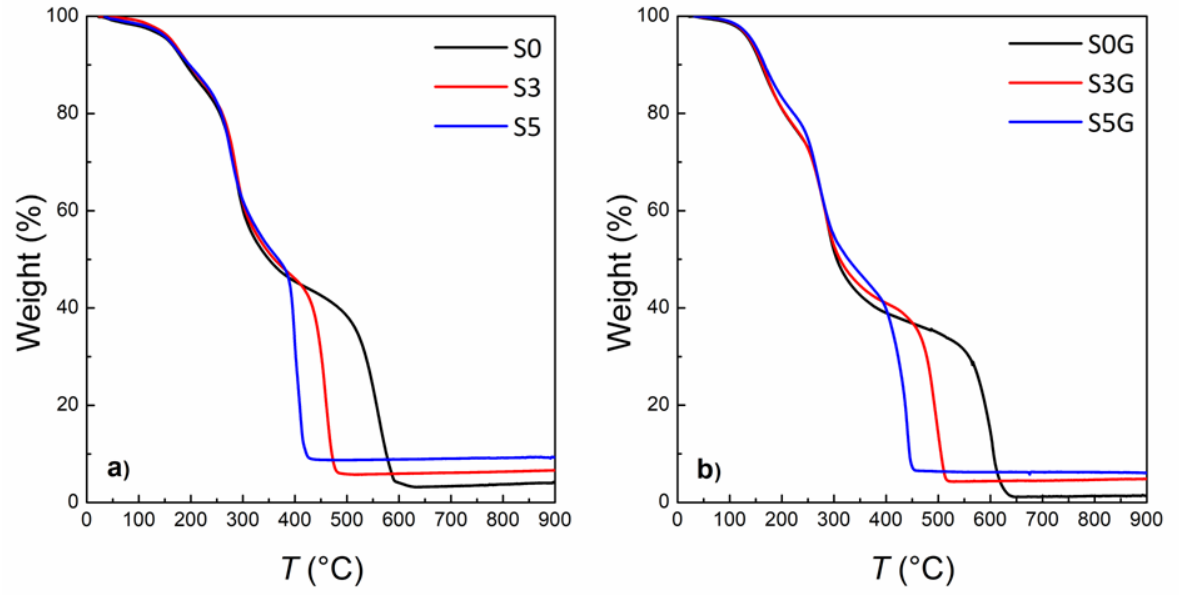

Figure 2. TGA curves of nanocomposite films: (a) non-plasticized; (b) containing 30 wt.% glycerol.

The direct observation of the non-plasticized and plasticized films (images not shown) denotes that the samples become darker with the increase of the content of iron oxides, due to the strong coloration of the added magnetic particles. However, inhomogeneous color was detected, indicating the existence of zones with more concentration of magnetic solute. In comparison to other methods, the synthesis protocol used in this work to incorporate MNP into the matrices (synthesis of MNP and posterior dispersion by sonication in the film forming solution), seems to promote the cluster formation, resulting in lesser homogeneous films, when they are compared to those synthesized using"*in situ*" procedures [25,52].

FESEM analysis was performed to characterize the morphology of the composites. Figure 3 shows images from the cross section of plasticized and non-plasticized films obtained by fragile fracture under liquid air. Different sizes of structures related to iron oxide particles can be observed, ranging from small agglomerates to relatively large clusters formed by collapsed individual particles. As expected, the images show a clear increase in density of white particles (associated to dispersed magnetic entities) as the content of particles increases. On the other hand, although the images presented in Figure 3 seem to denote bigger structures for the plasticized films, the technique did not allow determining an unequivocal trend regarding the size of agglomerates.

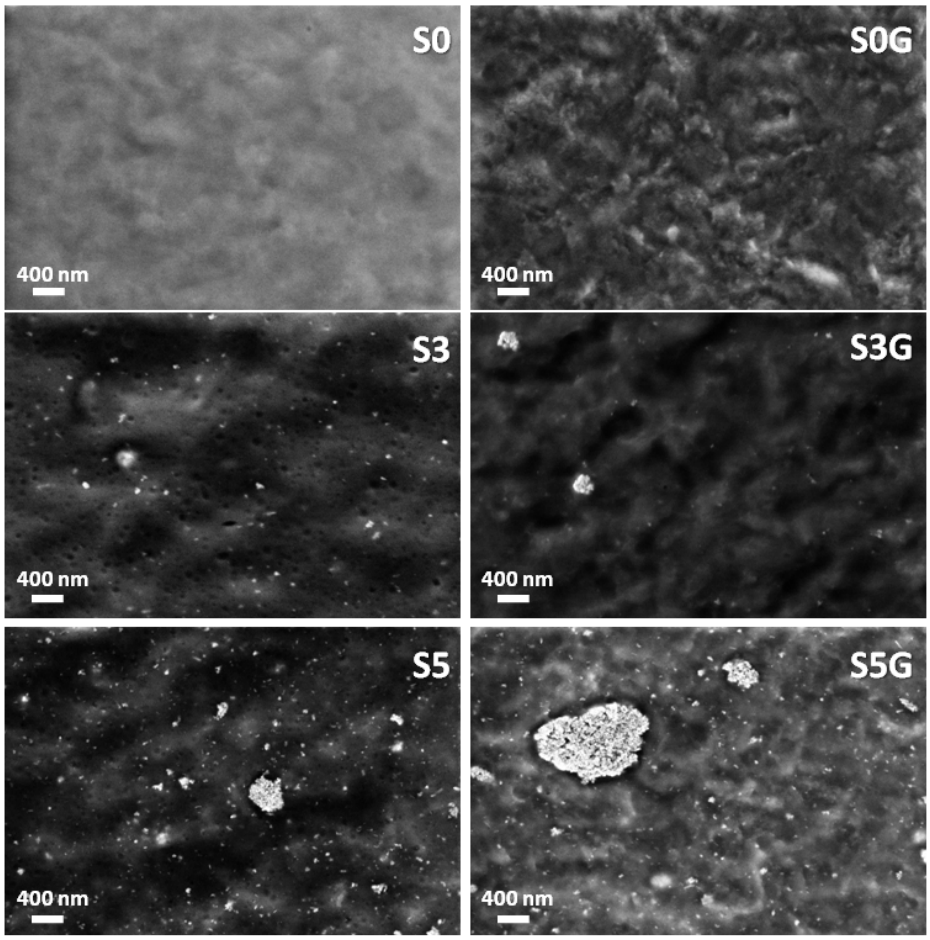

Figure 3. FESEM micrographs of the nanocomposites for three selected films.

Tensile properties of the films are summarized in Table 2. Both, modulus and strength of the non-plasticized films increase with the increment of MNP content. As an example, the addition of MNP into non-plasticized matrix in the sample S5 generates a 52.8% of increase in the modulus and 37% in the ultimate stress respect to the neat matrix. The increase of modulus is related with the high rigidity of the MNP in comparison with that of the polymeric matrix and can be expected if the particles or their clusters are homogeneously distributed and no pores or bubbles are generated during drying of the composite. On the other hand, the increase in ultimate stress of nanocomposites in comparison with that of the neat matrix is expected only when the filler acts as reinforcement, which normally takes place for fillers highly compatible and/or interacting with the polymeric matrix [53,54]. Anyhow, the standard deviation of both measurements is high for some of the samples and thus probably the unique significant difference can be found by comparing S5 composite with the neat matrix.

Table 2. Tensile properties of the films.

Sample	**E (MPa)**	**σ_u (MPa)**	**ε_b (%)**
S0	1098 ± 337^{b}	22.7 ± 7.6^{a}	14.8 ± 11.6^{a}
S1	1215 ± 328^{b}	25.8 ± 6.4^{a}	17.5 ± 11.6^{a}
S2	1025 ± 509^{b}	27.5 ± 6.1^{a}	11.6 ± 5.3^{a}
S3	1229 ± 46^{b}	27.9 ± 3.3^{a}	11.9 ± 6.1^{a}
S4	1482 ± 401^{ab}	30.4 ± 9.4^{a}	14.1 ± 7.3^{a}
S5	1677 ± 108^{a}	31.1 ± 4.3^{a}	11.3 ± 6.3^{a}

S0G	69 ±14^{c}	7.5 ± 1.9^{bc}	15.5 ± 5.1^{a}
S1G	73 ± 14^{c}	5.2 ± 0.8^{c}	8.6 ± 2.4^{a}
S2G	79 ± 16^{c}	5.6 ± 1.6^{bc}	8.6 ± 2.9^{a}
S3G	77 ± 15^{c}	8.3 ± 2.1^{b}	12.1 ± 2.3^{a}
S4G	60 ± 14^{c}	7.1 ± 1.5^{bc}	14.3 ± 0.9^{a}
S5G	79 ± 22^{c}	7.7 ± 3.3^{bc}	12.5 ± 6.5^{a}

^{a,b,c} Different letters in the same column indicate significant differences ($p < 0.05$). Reported values correspond to the mean ± standard deviation.

Pukanszky and co-workers [55] assumed that the yield stress of a filled polymer is determined by the decrease of the effective load bearing cross section of the matrix due to filler and by the polymer-filler interaction. They proposed the following equation to relate the strength of the particulate composite with the volume fraction of filler:

$$\sigma_{film} = \sigma_{matrix}\left(\frac{1 - V_{MNP}}{1 + 2.5 \cdot V_{MNP}}\right) \cdot exp(B \cdot V_{MNP}) \quad (1)$$

where σ_{film} and σ_{matrix} are the ultimate stresses of the nanocomposite film and the unfilled matrix, respectively, V_{MNP} is the volume fraction of the magnetic solute into the film (MNP in this case) and B is a parameter related with the specific area and density of the filler as well as the thickness and strength of the interface characterizing the interfacial interaction filler-matrix, which serve also as a measurement of the reinforcement efficiency of the filler [40].

If $B = 0$ the filler acts as a void and no adhesion and no stress transfer take place at the filler-matrix interface. For $B > 3$ the filler-matrix interface is good, and an effective reinforcing effect is obtained.

The volume fraction of MNP (V_{MNP}) can be calculated, assuming additivity of the volumes (v) as follow:

$$V_{MNP} = \frac{v_{MNP}}{v_{film}} = \frac{\frac{W_{MNP}}{\rho_{MNP}}}{\frac{W_{MNP}}{\rho_{MNP}} + \frac{W_{matrix}}{\rho_{matrix}}} \quad (2)$$

The density of the unfilled matrix (ρ_{matrix}=1.3 g/cm^3) was experimentally determined as the ratio between the weight and volume of a rectangular specimen, and the density of the filler (ρ_{MNP}) was taken as 5.175 g/cm^3 [56].

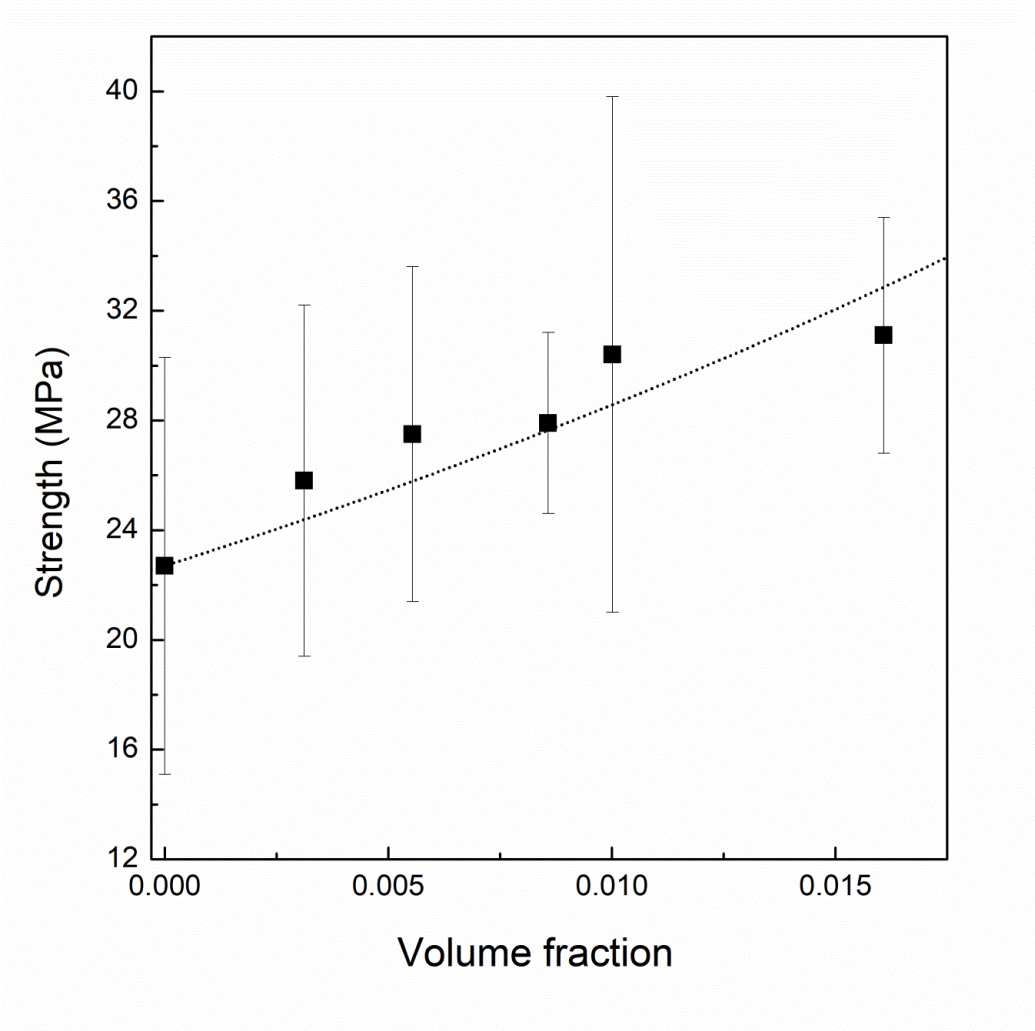

Figure 4. Experimental (symbols) strength and theoretical (dash line) values calculated from the Pukanszky model as a function of MNP volume fraction.

Figure 4 shows the evolution of the ultimate stress as function of volume fraction of MNP for non-plasticized films. In the same figure, the calculated fitting curve (equation 1) is displayed. According to the fit results, a value of 26 was found for the *B* parameter, being this much larger than 3, meaning that the interface is strong and an effective reinforcing effect was obtained [57].

On the other hand, the strong plasticizing effect of the glycerol is clearly denoted by the important decrease of the rigidity of plasticized samples with respect to non-plasticized ones, resulting in lower modulus and strength values (Table 2). However, these properties do not present a clear trend with MNP concentration. Particle agglomeration could affect the effective stiffness of the particles and the load transfer at the matrix-particle interface, facts related with modulus and strength of the nanocomposites, respectively. This behavior could be attributed to the heterogeneity of the films regarding MNP concentration and probably associated with less compatibility between particles and plasticized matrix than the observed for the non-plasticized samples. This fact could be directly associated to the presence of higher agglomerates in the nanocomposites with glycerol as was previously mentioned in the analysis of FESEM images.

The ultimate deformation does not present a clear trend, neither with respect to magnetite concentration, nor with respect to glycerol content (i.e. comparing S samples with SG samples at fixed magnetite concentration).

From FESEM images analysis, it became clear that composite samples contain aggregates of individual particles. Thus, the SAXS technique was used to complement the

structural information, as well as to follow the cluster formation into the chitosan based films. The range of analysis of the SAXS measurements is restricted with respect to the size of particles or structures loaded into the matrix (i.e. depends on the selected q range). Here some general information about nanostructures will be obtained and used as a comparative tool. Firstly it should be noticed that even when the FESEM images suggest the presence of at least a bimodal distribution of cluster sizes, the measured q-range in SAXS covers those scattering objects matching the smaller ones.

Figure 5 shows the Log–Log representation of scattering intensity, I(q) versus the momentum transfer, q, for the magnetic nanocomposites. As can be noted, the SAXS experimental curves display similar trends, where three different scattering regions can be highlighted. In low-q region, all spectra exhibit similar power law trends, indicating a deviation from the Guinier behavior, characteristic of non-interacting individual particles (i.e. ultra-dispersed systems). This deviation can be attributed to the scattering interference between the neighboring iron oxide NPs, denoting their aggregation into the films [58,59]. In this zone (Guinier region), for q–values lower than 0.1 nm^{-1}, a power law of $I \sim q^{-2.4}$ was found for all samples. In the high-q region, the scattering intensity behavior can be described with a power law $I(q) \sim q^{-\beta}$, being β the Porod exponent, whose values were found between -3 and -4 for all samples, characteristic of Porod scattering from smooth and sharp interfaces among iron oxide NPs and polymer matrix [60–62]. At intermediate q-values ($0.2\ nm^{-1} < q < 0.95\ nm^{-1}$), the absence of oscillations suggests a moderate polydispersity of the MNP loaded into the chitosan matrices.

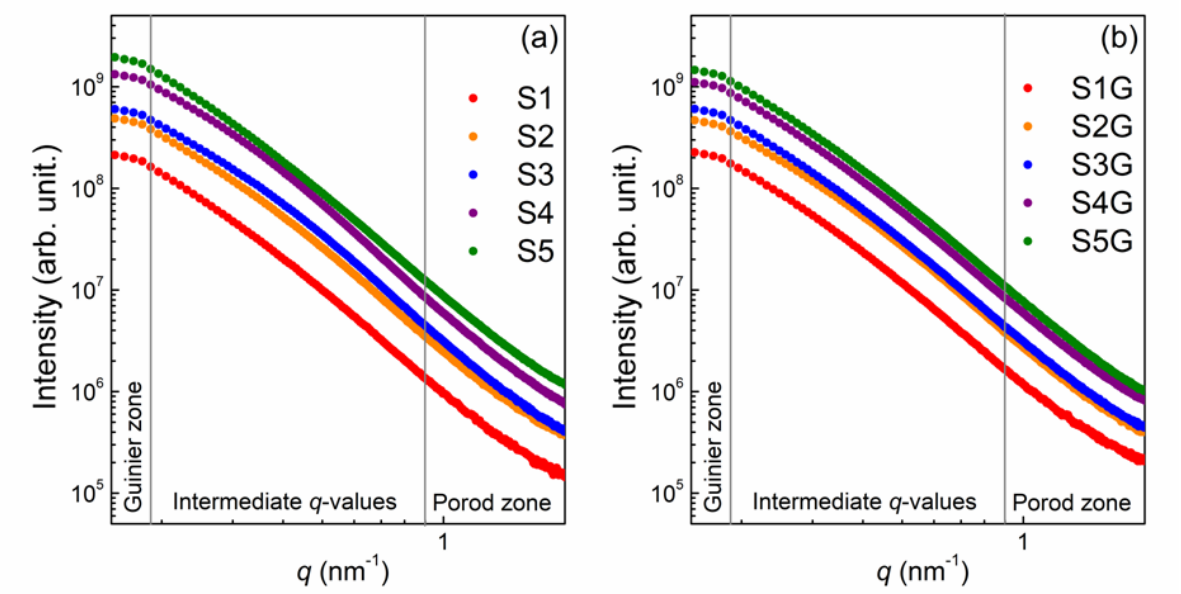

Figure 5. Small angle X-ray scattering intensity (I) as a function of the momentum transfer vector (q) for non-plasticized (a) and plasticized samples (b).

To perform a quantitative analysis, experimental SAXS curves were evaluated using the unified exponential/power-law postulated by Beaucage and based on hierarchical structures [63]. The phenomenology behind this model implies to consider a combination of the Porod and Guinier regimes to describe the scattering intensity of any systems composed by entities of complex morphology, which can contain multiple levels of related structural features. In our case, to describe two interconnected structural levels (aggregates and individual NPs), the following equation was used:

$$I(q) \cong G\, exp\frac{\left(-q^2 {R_g}^2\right)}{3} + B\, exp\frac{\left(-q^2 {R_s}^2\right)}{3}\left(\frac{\left(\mathrm{erf}\left(qR_g/\sqrt{6}\right)^3\right.}{q}\right)^{D_f} + Gs\, exp\frac{\left(-q^2 {R_s}^2\right)}{3} + Bs\left(\frac{\left(\mathrm{erf}\left(qR_s/\sqrt{6}\right)^3\right.}{q}\right)^{P} \qquad (3)$$

where G and B correspond to the Guinier and Porod pre-factors of those larger structures detected in the measured q range (aggregates); Gs and Bs are the Guinier and Porod pre-

factors of the smaller structures (individual particles); *Rg* is the radius of gyration of aggregates with fractal dimension *Df*, and whose architecture is defined by small particles of size *Rs*. *P* is the exponent of the power law assigned to the smaller structures and *erf* is the error function. Notice that the first term of equation 3 describes the large-scale structure of size *Rg*, while the second one refers to the mass-fractal regime with two structural limits. The last two terms are related with the structural information of smaller substructure (primary MNPs).

The Beaucage approach was successfully applied to describe the scattering intensity from those polydispersed NPs that interact forming clusters of larger sizes into the selected matrices. The curves obtained by fitting the model are in good agreement with experimental data, as can be observed in Figure 6 for the samples S1, S5, S1G and S5G. The individual contributions of the Guinier and Porod component curves of aggregates (curves 1 and 2) and primary particles (curves 3 and 4) are also included in the plot (dashed lines).

Thus, equation 3 allows modeling the experimental SAXS results and determining the fitting parameters, such as *Rg*, *Df* and the pre-factors, *G*, *B*, *Gs* and *Bs* for different chitosan/MNP films (Table 4). The *P* exponent and the single nanoparticle radius (*Rs*) were set as 4 and 4.8 nm (this last one, according to TEM information), respectively, although a relative small variation of ±10% was allowed for fitting purposes.

Fitting parameters *G*, *B*, *Gs* and *Bs* (see Table 4) increase with MNP content for both, plasticized and non-plasticized samples as was expected, because they are directly related with the relative amount of iron oxide NPs (*Gs* and *Bs*) and agglomerates (*G* and *B*). As the amount of individual particles rises, an increase in the amount of agglomerates is expected. In addition, the pre-factors are higher for the non-plasticized samples with the most important differences in *G* and *B* parameters, fact that could be related with

differences in the electronic contrast between the matrix and particles, when the former is plasticized or not: the presence of glycerol can modify the dispersion length densities of the matrix and consequently the electronic contrast of particular zones of the composite.

Table 4 also presents the polydispersity index, PDI, and the grade of aggregation, Z (defined as the amount of particles of mean radius *Rs* contained by an aggregate of radius *Rg*) calculated by the following equations [64].

$$PDI = \frac{Bs \cdot {R_s}^4}{1.62 \cdot Gs} \quad (4)$$

$$Z = \left(\frac{R_s}{R_g}\right)^{-D_f/2} \quad (5)$$

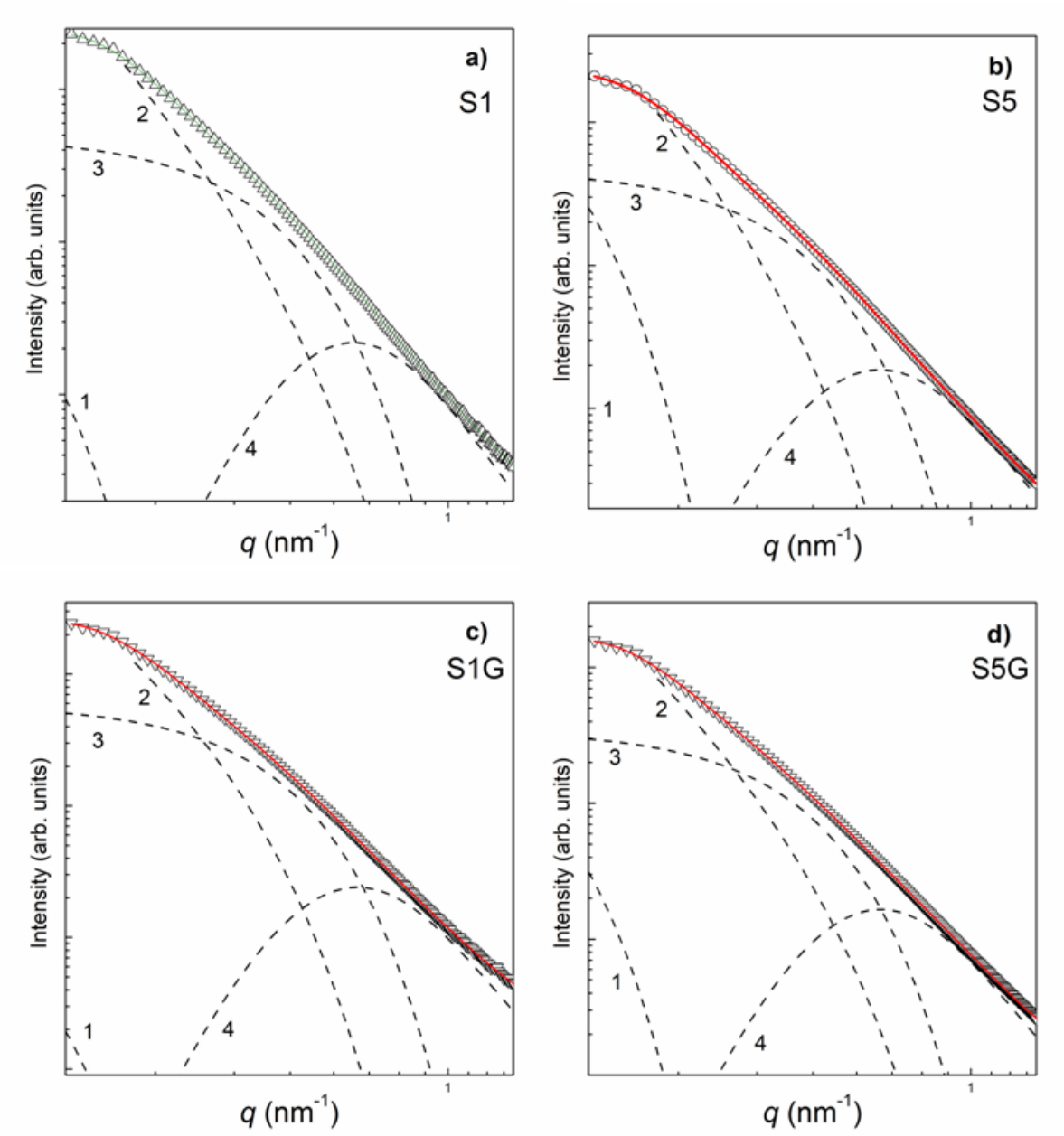

Figure 6. Experimental data (empty circles) and fitting of equation 3 with SASfit package (solid line) and the different contributions of Beaucage model. 1) Guinier aggregates, 2) Porod aggregates, 3) Guinier individual particles, 4) Porod individual particles.

Since *Df* is a parameter of the fractal dimension, their values, quite similar for all films, indicate that in all the samples the agglomerates of individual particles have similar structures. Their values are mostly close to 3, indicating tridimensional smooth and compact clusters [65] with a tridimensional architecture. On the other hand, *Rg*, which stands for the aggregate sizes, does not suffer significant variation with the concentration of MNP. Assuming that the shape of the agglomerates is spherical, their sizes can be calculated using $\xi = 2(5/3)^{1/2}Rg$.

Table 4. SAXS parameters obtained using equations 3-5.

G: Guinier pre-factor of larger structures, B: Porod pre-factor of larger structures, Gs: Guinier pre-factor of smaller structures, Bs: Porod pre-factor of the smaller structures, Rg: radius of gyration of aggregates, Df: fractal dimension, Rs: radius of individual particles, P: exponent of the power law assigned to the smaller structures, ξ: radius of the agglomerate, PDI: polydispersity index, Z: grade of aggregation.

Sample	G	B	Gs	Bs	Rg (nm)	Rs (nm)	Df	P	ξ (nm)	PDI	Z
S1	5.03E7	1.22E6	4.47E7	8.88E5	21.92	4.792	2.99	4.01	55.56	6.3	19.1
S2	2.24E7	2.95E6	1.20E8	2.38E6	21.51	4.757	2.98	3.82	55.55	6.3	17.8
S3	1.69E7	3.79E6	1.55E8	2.95E6	21.79	4.770	2.92	3.99	56.26	6.1	20.8
S4	6.89E8	2.10E7	3.37E8	5.62E6	21.17	4.795	2.46	3.98	54.65	5.5	19.1
S5	4.95E9	1.16E7	3.87E8	8.60E6	21.04	4.776	2.99	3.72	51.43	6.1	13.8
S1G	3.77E6	2.84E6	5.87E7	1.05E6	21.317	4.795	2.61	3.98	55.04	5.8	19.5
S2G	2.70E8	3.43E6	1.34E8	2.53E6	21.11	4.795	2.88	3.98	54.51	6.2	19.1
S3G	2.80E8	3.38E6	1.40E8	2.89E6	21.38	4.794	3.04	3.98	55.20	6.7	19.5
S4G	5.31E8	6.23E6	2.65E8	5.55E6	21.16	4.793	3.04	3.97	54.63	6.8	19.0

S5G	6.08E8	7.82E6	3.45E8	7.26E6	21.30	4.792	3.06	3.97	55.00	6.8	19.3

Figure 7 shows a general overview of the DC magnetic properties in the investigated nanocomposite films. The temperature dependende of magnetization for different samples is displayed in Figures 7 (a) and (d); these curves were recorded at a low DC field of 50 Oe under the zero-field-cooling and field-cooling protocols. As can be noted, all the ZFC/FC curves show a similar behavior, where the *ZFC* magnetization curves progressively increases without a defined maximum in the range of analyzed temperatures, while, the *FC* curves show a monotonous decrease as temperature rises. Moreover, *ZFC* and *FC* joint near to 300 K, which indicates that both blocking and irreversibility temperatures are probably close to room temperature. These are characteristics for highly or moderate interacting nanoparticulated systems, with a broad size distribution and where not all the NPs become unblocked at 300 K [66].

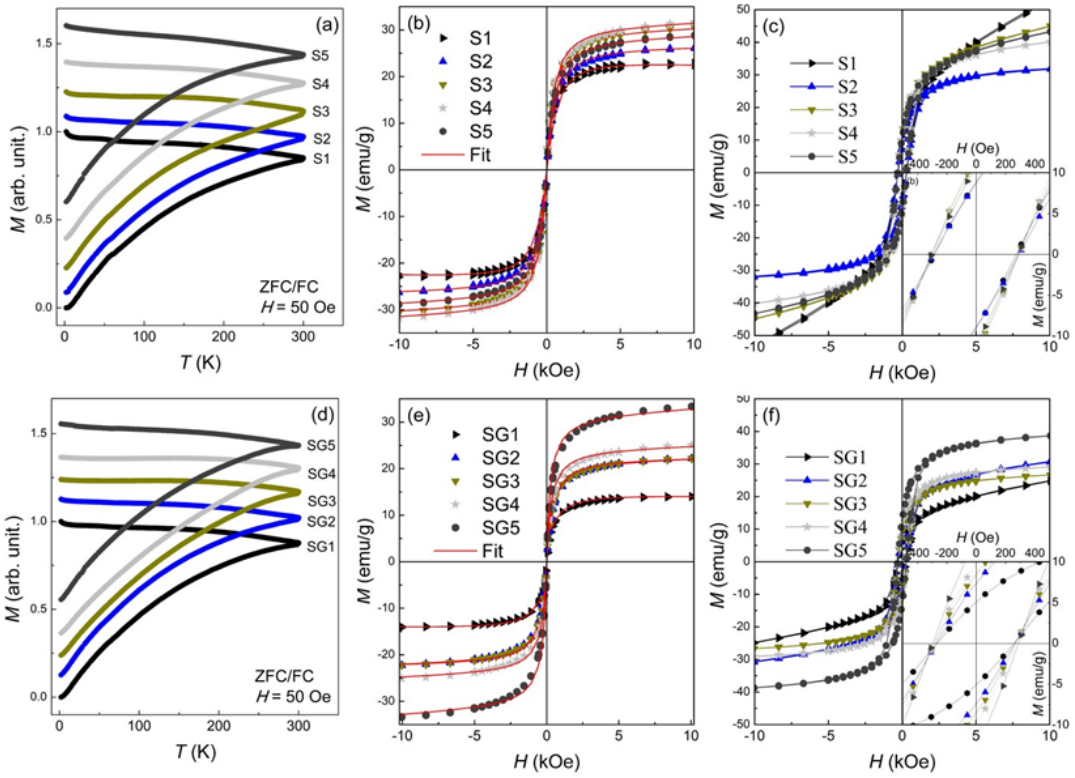

Figure 7. (a) and (d) Magnetization as a function of the temperature recorded under *ZFC* and *FC* protocols for samples S and SG, respectively. *ZFC* and *FC* curves are normalized and vertically displaced for better understanding. (b) and (c) Magnetization vs. magnetic field curves at 300 and 2 K for samples S. (e) and (f) Magnetization vs. magnetic field curves at 300 and 2 K for samples SG. Continuous lines at *M* vs.*H* recorded at 300 K represent the Langevin fits. Magnetization values are presented in emu/g of magnetic material.

Isothermal hysteresis loops were measured in all nanocomposites at two different temperatures (2 K and 300 K). According to our results, every *M* vs. *H* curve obtained at

300 K (Figures 7(b) and (e)) displays a *S*-shape with an almost null coercive field (*H*c) i.e., absence of hysteresis. This is a typical feature of granular systems composed by monodomain NPs, as explained by Allia et al [67] and Knobel et al [68]. Besides, the magnetization values obtained at 2K are larger than the ones measured at 300K. Despite that the magnetization curves of both systems (plasticized and not plasticized) share some similarities, there are differences in the magnetization saturation (*M*s) values. For instance, comparing the *M* vs. *H* curves measured at 300K, those films loaded with lowest NP concentrations, i.e., S1 and SG1, take values of *Ms* around ~21 emu/g and 18 emu/g (normalized per MNP mass), respectively. On the other hand, in samples S5 and SG5 (nanocomposites films with highest NP concentration), the *Ms* have values of 27 and 35 emu/g, respectively. Thus, for both sets of analyzed magnetic nanocomposite films one can distinguish an increase of M_S as the concentration of magnetic solute rises from samples 1 to 5.

This behavior seems to be dependant on the NPs concentration, where aggregates features, such as size and compactness degree, are directly influenced by the amount of magnetic solute (as was inferred from SAXS and FESEM analysis). In addition, the aggregate formations lead to different collective behaviors among NPs, which should be related to cluster features. These facts can reveal the formation of systems with differences in dipolar interactions and effective anisotropies, which affect the magnetization dynamics, consequently, the corresponding macroscopic parameters (such as M_S and/or H_C) [69]. It is worth noting that all the *M* vs. *H* curves display lower values of M_S, when compared to those reported for bulk magnetite [70]. This behavior can be understood considering the disorder on the nanoparticle surface [71]. Comparing the magnetization behavior of the two sets of systems, differences between the M_S values of samples S and SG for a specific

concentration can easily perceived, suggesting different aggregation of the NPs. This effect can be affected by the interaction among the functional groups of the matrix and the active chemical groups located at the interface of the nanoparticle, as suggested in previous works [52,72]. Table 5 listes the coercive field values (*H*c) extracted from the *M* vs. *H* curves obtained at 2K. For both systems (S and SG) it can be noticed that H_C tends to higher values as the temperature decrease, which is an experimental evidence that the NPs are in the blocked regime at 2 K consistent with ZFC and FC results [59,73]. Furthermore, for each nanoparticle concentration, lower values of H_C can be observed for plasticized samples (SG) in comparison to the other ones. This behavior could indicate the formation of aggregates with low compactness degree.

In order to perform a quantitative analysis of the above discussed facts, we applied the Langevin formulation to fit the *M* vs. *H* curves measured at 300 K. Briefly, the magnetization response as a function of the magnetic field for granular nanoparticle systems can be described by the Langevin function $M = M_S L(\mu H/k_B T)$, being μ the magnetic moment per monodomain entity, k_B the Boltzmann constant and M_S the saturation magnetization, that also can be expressed as $M_S = N\mu$, *N* being the number of monodomain entities per unit mass. To take into account the moment distribution (related to the presence of a particle size distribution), Langevin function was weighted by a lognormal distribution function $f(\mu)$ with median μ_M ($= \mu \exp(\sigma^2/2)$), being σ the standard deviation. Then, the *M* vs. *H* data were fitted by:

$$M(H) = N\int_0^\infty \mu L\left(\frac{\mu H}{k_B T}\right) f(\mu) d\mu + C, \qquad (6)$$

where the last term C is a constant that contains the paramagnetic contributions that come from the nanoparticle surface disorder. The fitted curves are displayed as full lines in

Figures 7 ((b) and (e)) and the fitted parameters are summarized in Table 5. To interpret the fitting results, it must be considered that the framework behind the Langevin formulation is based on ideal systems, i.e., non-interacting and monodomain entities with moderate size distribution. However, a reinterpretation of the obtained results can support the hypothesis that the formation of aggregates with different features (each one acting as a magnetic entity) dominates the magnetization response. Accordingly, the obtained parameters, σ and N, do not vary widely, while for the two investigated sets of samples, the mean magnetic moment per magnetic entity (μ_M) present an increase as the nanoparticle concentration increase; for instance, μ_M of 11.8 μ_B and 6.7 μ_B were obtained for samples S1 and S1G, respectively, while for the most concentrated samples (S5 and S5G), values of 12.5 μ_B and 14.3 μ_B were found. The observed variance of μ_M can be understood from the NP arrangement (size and compactness degree) that forms each aggregate.

On samples with lower magnetic solute, it seems that the NPs are randomly arranged to give rise to structures of shorter magnetic size. On the contrary, in samples with high nanoparticle concentration, it seems that the NPs that form the aggregates are organized so that their magnetic moments are forming cooperative magnetic systems, leading to more compact structures with a bigger net magnetic moment. Theses hypothesis could suggest a cooperative-type arrangement of those magnetic moments that belong to the percolated NPs (high nanoparticle concentrations). Such hypothesis also implies that for larger NP concentration, the super-paramagnetic features of the system can be lost, which result in a magnetic response governed by the aggregates characteristics.

Table 5. Best fitting parameters according to equation 6 and coercive fields obtained from the *M* vs. *H* curves recorded at 2K.

σ: variance, $\mu_{M:}$ magnetic moment per magnetic entity, N the number of monodomain entities per unit mass, Hc: coercive field

Sample	σ	μ_M ($10^3\mu_B$)	N (10^{17}cm^{-3})	Hc (Oe) at 2 K
S1	0.3	11.8	2.2	280
S2	0.4	11.9	2.1	290
S3	0.6	12.4	2.2	295
S4	0.6	12.6	2.2	298
S5	0.5	12.5	2.2	297
SG1	1.0	6.7	1.5	260
SG2	0.8	10.7	1.6	265
SG3	0.8	11.1	1.6	276
SG4	0.8	13.1	1.4	278
SG5	0.9	14.3	1.6	290

4 CONCLUSIONS

A procedure to obtain magnetic nanocomposite films using a bio-polymeric matrix (chitosan) and magnetic nanoparticles was reported. The nanoparticles of iron oxides were synthesized by an alkaline co-precipitation method that leads to the formation of magnetite and/or maghemite particles of less than 10 nm average diameter. FESEM micrographs, tensile tests, magnetic properties and SAXS analysis were used to evaluate film specific properties, but also to obtain indirect information regarding film's nano and microstructure.

The mechanical behavior under uniaxial tensile tests was associated to a good interaction nanoparticles-matrix, mainly for the non-plasticized samples where a clear reinforcing effect was observed.

Magnetic results showed that the nanoparticles within the films are super-paramagnetic, with blocking temperatures close to room temperature. Generally speaking, the magnetic response was dominated by the collective behavior of interacting dipolar nanoparticles associated with the presence of aggregates with variations in sizes and compactness degree. The aggregation of individual magnetic particles in the composite films was corroborated from FESEM images, with the larger ones found in the plasticized samples. SAXS data were successfully fitted with the Beaucage model and the calculated parameters denoted the existence of volume fractal dimensions in the smaller clusters.

In conclusion, these nanocomposites are excellent candidates for a wide range of applications, owing to (i) easy access and low cost of raw materials and processing, (ii) the low toxicity of chitosan, MNP and the solvent used (water), (iii) the chelating characteristics inherent to chitosan and magnetic nanoparticles.

ACKNOWLEDGEMENTS

The authors gratefully acknowledge the financial support provided by the National Research Council of Argentina (CONICET, Grant PIP 112 201101 00866), the Science and Technology National Promotion Agency (ANPCyT, Grant PICT-2013-1535) and the National University of Mar del Plata (Project # 15/G430-ING 436/15). The work at UNICAMP was supported by FAPESP (2014/26672-8) and CNPq #303236/2017-5, Brazil. Small-angle X-ray scattering data were acquired at beamline SAXS1 (proposal 20160488) at Brazilian Synchrotron Light Laboratory (LNLS). The authors also acknowledge to the Brazilian Nanotechnology National Laboratory (LNNano) for the use of TEM facilities.

DATA AVAILABILITY

The raw/processed data required to reproduce these findings cannot be shared at this time as the data also forms part of an ongoing study.

REFERENCES

[1] S.M. Husnain, W. Um, Magnetite-based adsorbents for sequestration of radionuclides : a review, RSC Advances. 8 (2018) 2521–2540. doi:10.1039/C7RA12299C.

[2] N.A. Pattanashetti, G.B. Heggannavar, M.Y. Kariduraganavar, Smart biopolymers and their biomedical applications, Procedia Manufacturing. 12 (2017) 263–279. doi:10.1016/j.promfg.2017.08.030.

[3] D.W. Cho, B.H. Jeon, C.M. Chon, Y. Kim, F.W. Schwartz, E.S. Lee, H. Song, A novel chitosan/clay/magnetite composite for adsorption of Cu(II) and As(V), Chemical Engineering Journal. 200–202 (2012) 654–662. doi:10.1016/j.cej.2012.06.126.

[4] E. Alver, M. Bulut, H. Çiftçi, Molecular and biomolecular spectroscopy one step effective removal of Congo Red in chitosan nanoparticles by encapsulation, Spectrochimica Acta Part A. 171 (2017) 132–138.

[5] M. Agostini de Moraes, D.S. Cocenza, F. da Cruz Vasconcellos, L.F. Fraceto, M.M. Beppu, Chitosan and alginate biopolymer membranes for remediation of contaminated water with herbicides, Journal of Environmental Management. 131 (2013) 222–227. doi:10.1016/j.jenvman.2013.09.028.

[6] A. Rafiee, M.H. Alimohammadian, T. Gazori, F. Riazi-rad, S.M.R. Fatemi, A. Parizadeh, I. Haririan, M. Havaskary, Comparison of chitosan, alginate and

chitosan/alginate nanoparticles with respect to their size, stability, toxicity and transfection, Asian Pacific Journal of Tropical Disease. 4 (2014) 372–377. doi:10.1016/S2222-1808(14)60590-9.

[7] A.F. Martins, P.V.A. Bueno, E.A.M.S. Almeida, F.H.A. Rodrigues, A.F. Rubira, E.C. Muniz, Characterization of N-trimethyl chitosan/alginate complexes and curcumin release, International Journal of Biological Macromolecules. 57 (2013) 174–184. doi:10.1016/j.ijbiomac.2013.03.029.

[8] G.L. Dotto, V.C. de Souza, J.M. de Moura, C.M. de Moura, L.A. de Almeida Pinto, Influence of drying techniques on the characteristics of chitosan and the quality of biopolymer films, Drying Technology. 29 (2011) 1784–1791. doi:10.1080/07373937.2011.602812.

[9] K. Yu, J. Ho, E. McCandlish, B. Buckley, R. Patel, Z. Li, N.C. Shapley, Copper ion adsorption by chitosan nanoparticles and alginate microparticles for water purification applications, Colloids and Surfaces A: Physicochemical and Engineering Aspects. 425 (2013) 31–41. doi:10.1016/j.colsurfa.2012.12.043.

[10] H.V. Tran, L.D. Tran, T.N. Nguyen, Preparation of chitosan/magnetite composite beads and their application for removal of Pb(II) and Ni(II) from aqueous solution, Materials Science and Engineering C. 30 (2010) 304–310. doi:10.1016/j.msec.2009.11.008.

[11] P. Xu, G.M. Zeng, D.L. Huang, C.L. Feng, S. Hu, M.H. Zhao, C. Lai, Z. Wei, C. Huang, G.X. Xie, Z.F. Liu, Use of iron oxide nanomaterials in wastewater treatment: A review, Science of the Total Environment. 424 (2012) 1–10. doi:10.1016/j.scitotenv.2012.02.023.

[12] K.J. Sreeram, M. Nidhin, B.U. Nair, Synthesis of aligned hematite nanoparticles on

chitosan-alginate films, Colloids and Surfaces B: Biointerfaces. 71 (2009) 260–267. doi:10.1016/j.colsurfb.2009.02.015.

[13] F. Zhuang, R. Tan, W. Shen, X. Zhang, W. Xu, W. Song, Magnetic strontium hydroxyapatite microspheres for the efficient removal of Pb (II) from acidic solutions, Journal of Chemical & Engineering Data. 59 (2014) 3873–3881.

[14] A.E. Regazzoni, G.A. Urrutia, M.A. Blesa, A.J.G. Maroto, Some observations on the composition and morphology of synthetic magnetites obtained by different routes, Journal of Inorganic and Nuclear Chemistry. 43 (1981) 1489–1493. doi:10.1016/0022-1902(81)80322-3.

[15] D.J. Shaw, Introduction to Colloid and Surface Chemistry, Butterworth Heinemann (a division of Reed Educational and Professional Publishers), Woburn, USA, 1992.

[16] M. Lavorgna, F. Piscitelli, P. Mangiacapra, G.G. Buonocore, Study of the combined effect of both clay and glycerol plasticizer on the properties of chitosan films, Carbohydrate Polymers. 82 (2010) 291–298. doi:10.1016/j.carbpol.2010.04.054.

[17] A. Zhu, L. Yuan, T. Liao, Suspension of Fe3O4 nanoparticles stabilized by chitosan and o-carboxymethylchitosan, International Journal of Pharmaceutics. 350 (2008) 361–368. doi:10.1016/j.ijpharm.2007.09.004.

[18] F. Cesano, G. Fenoglio, L. Carlos, R. Nisticò, One-step synthesis of magnetic chitosan polymer composite films, Applied Surface Science. 345 (2015) 175–181.

[19] O. Bezdorozhev, T. Kolodiazhnyi, O. Vasylkiv, Precipitation synthesis and magnetic properties of self-assembled magnetite-chitosan nanostructures, Journal of Magnetism and Magnetic Materials. 428 (2017) 406–411. doi:10.1016/j.jmmm.2016.12.048.

[20] J. Singh, M. Srivastava, J. Dutta, P.K. Dutta, Preparation and properties of hybrid

monodispersed magnetic ??-Fe2O3 based chitosan nanocomposite film for industrial and biomedical applications, International Journal of Biological Macromolecules. 48 (2011) 170–176. doi:10.1016/j.ijbiomac.2010.10.016.

[21] A.S. Bhatt, D. Krishna Bhat, M.S. Santosh, Electrical and magnetic properties of chitosan-magnetite nanocomposites, Physica B: Condensed Matter. 405 (2010) 2078–2082. doi:10.1016/j.physb.2010.01.106.

[22] M. Knobel, L.M. Socolovsky, J.M. Vargas, Propiedades magnéticas y de transporte de sistemas nanocristalinos : conceptos básicos y aplicaciones a sistemas reales, Revista Mexicana de Física. 50 (2004) 8–28.

[23] R. Fu, Y. Yan, C. Roberts, Z. Liu, Y. Chen, The role of dipole interactions in hyperthermia heating colloidal clusters of densely-packed superparamagnetic nanoparticles, Scientific Reports. 8 (2018) 1–10. doi:10.1038/s41598-018-23225-5.

[24] G.A. Kloster, D. Muraca, C. Meiorin, K.R. Pirota, N.E. Marcovich, M.A. Mosiewicki, Magnetic characterization of chitosan – magnetite nanocomposite films, European Polymer Journal. 72 (2015) 202–211. doi:10.1016/j.eurpolymj.2015.09.014.

[25] G.A. Kloster, N.E. Marcovich, M.A. Mosiewicki, Composite films based on chitosan and nanomagnetite, European Polymer Journal. 66 (2015) 386–396. doi:10.1016/j.eurpolymj.2015.02.042.

[26] R. Massart, V. Cabuil, Synthèse en milieu alcalin de magnétite colloïdale: contrôle du rendement et de la taille des particules, Journal de Chimie Physique. 84 (1987) 967–973.

[27] C. Meiorin, D. Muraca, K.R. Pirota, M.I. Aranguren, M.A. Mosiewicki, Nanocomposites with superparamagnetic behavior based on a vegetable oil and

magnetite nanoparticles, European Polymer Journal. 53 (2014) 90–99. doi:10.1016/j.eurpolymj.2014.01.018.

[28] Y. Peng, C. Park, J. Zhu, R.M. White, D.E. Laughlin, Y. Peng, C. Park, J. Zhu, R.M. White, D.E. Laughlin, Characterization of interfacial reactions in magnetite tunnel junctions with transmission electron microscopy, Journal of Applied Physics. 95 (2004) 6798–6800. doi:10.1063/1.1688535.

[29] L. Zhang, R. He, H. Gu, Oleic acid coating on the monodisperse magnetite nanoparticles, Applied Surface Science. 253 (2006) 2611–2617. doi:10.1016/j.apsusc.2006.05.023.

[30] G. Schmid, Nanoparticles: From Theory to Application, Second, Wiley, 2005.

[31] M. González, I. Martín-fabiani, J. Baselga, J. Pozuelo, Magnetic nanocomposites based on hydrogenated epoxy resin, Materials Chemistry and Physics. 132 (2012) 618–624. doi:10.1016/j.matchemphys.2011.11.077.

[32] P. Scherrer, Göttinger nachrichten gesell, Journal of Mathematical Physics. 2 (1918) 98.

[33] A.R. Lang, X-ray diffraction procedures for polycrystal-line and amorphous materials, Acta Metallurgica. 4 (1956) 102. doi:10.1016/0001-6160(56)90124-9.

[34] A.L. Patterson, The Scherrer formula for X-ray particle size determination, Physical Review. 56 (1939) 978.

[35] A. Labarta, X. Batlle, O. Iglesias, Surface Effects in Magnetic Nanoparticles, Springer Science & Business Media, New York, 2005. doi:10.1017/CBO9781107415324.004.

[36] A. V Teixeira, I. Morfin, P. Panine, P. Licinio, E. Geissler, Structure and magnetic properties of dilute ferrofluids suspended in gels, Composites Science and

Technology. 63 (2003) 1105–1111. doi:10.1016/S0266-3538(03)00031-9.

[37] O. Kratky, G. Porod, Die Abhängigkeit der Röntgen-Kleinwinkelstreuung von Form und Grösse der kolloiden Teilchen in verdünnten Systemen: III, Acta Physica Austriaca. 2 (1948) 133.

[38] K. Cendrowski, P. Sikora, B. Zielinska, E. Horszczaruk, Chemical and thermal stability of core-shelled magnetite nanoparticles and solid silica, Applied Surface Science. 407 (2017) 391–397. doi:10.1016/j.apsusc.2017.02.118.

[39] E.R. Monazam, R.W. Breault, R. Siriwardane, Kinetics of magnetite (Fe3O4) oxidation to hematite (Fe2O3) in air for chemical looping combustion, Industrial and Engineering Chemistry Research. 53 (2014) 13320–13328. doi:10.1021/ie501536s.

[40] S.F. Wang, L. Shen, Y.J. Tong, L. Chen, I.Y. Phang, P.Q. Lim, T.X. Liu, Biopolymer chitosan / montmorillonite nanocomposites : Preparation and characterization, Polymer Degradation and Stability. 90 (2005) 123–131. doi:10.1016/j.polymdegradstab.2005.03.001.

[41] M. V. Debandi, C. Bernal, N.J. Francois, Development of biodegradable films based on chitosan/glycerol blends suitable for biomedical applications, Journal of Tissue Science & Engineering. 07 (2016). doi:10.4172/2157-7552.1000187.

[42] J.F. Fundo, A.C. Galvis-Sanchez, I. Delgadillo, C.L.M. Silva, M.A.C. Quintas, The effect of polymer/ plasticiser ratio in film forming solutions on the properties of chitosan films, Food Biophysics. 10 (2015) 324–333. doi:10.1007/s11483-015-9394-3.

[43] S. Rivero, M.A. García, A. Pinotti, Correlations between structural, barrier, thermal and mechanical properties of plasticized gelatin films, Innovative Food Science and Emerging Technologies. 11 (2010) 369–375. doi:10.1016/j.ifset.2009.07.005.

[44] K. Okuyama, K. Noguchi, T. Miyazawa, T. Yui, K. Ogawa, Molecular and crystal structure of hydrated chitosan, Macromolecules. 30 (1997) 5849–5855. doi:10.1021/ma970509n.

[45] G.D. Soto, C. Meiorin, D. Actis, P. Mendoza Zélis, M.A. Mosiewicki, N.E. Marcovich, Nanocomposites with shape memory behavior based on a segmented polyurethane and magnetic nanostructures, Polymer Testing. 65 (2018) 360–368. doi:10.1016/j.polymertesting.2017.12.012.

[46] V. Bertolino, G. Cavallaro, G. Lazzara, S. Milioto, F. Parisi, Halloysite nanotubes sandwiched between chitosan layers: Novel bionanocomposites with multilayer structures, New Journal of Chemistry. 42 (2018) 8384–8390. doi:10.1039/c8nj01161c.

[47] X.Q. Xu, H. Shen, J.R. Xu, M.Q. Xie, X.J. Li, The colloidal stability and core-shell structure of magnetite nanoparticles coated with alginate, Applied Surface Science. 253 (2006) 2158–2164. doi:10.1016/j.apsusc.2006.04.015.

[48] G.A. Kloster, D. Muraca, M.A. Mosiewicki, N.E. Marcovich, Magnetic composite fi lms based on alginate and nano-iron oxide particles obtained by synthesis " in situ ," European Polymer Journal. 94 (2017) 43–55.

[49] A. Moeini, A. Cimmino, G. Dal Poggetto, M. Di Biase, A. Evidente, M. Masi, P. Lavermicocca, F. Valerio, A. Leone, G. Santagata, M. Malinconico, Effect of pH and TPP concentration on chemico-physical properties, release kinetics and antifungal activity of Chitosan-TPP-Ungeremine microbeads, Carbohydrate Polymers. 195 (2018) 631–641. doi:10.1016/j.carbpol.2018.05.005.

[50] M. Ziegler-Borowska, D. Chełminiak, H. Kaczmarek, A. Kaczmarek-Kędziera, Effect of side substituents on thermal stability of the modified chitosan and its

nanocomposites with magnetite, Journal of Thermal Analysis and Calorimetry. 124 (2016) 1267–1280. doi:10.1007/s10973-016-5260-x.

[51] M. Ziegler-Borowska, D. Chełminiak, H. Kaczmarek, Thermal stability of magnetic nanoparticles coated by blends of modified chitosan and poly(quaternary ammonium) salt, Journal of Thermal Analysis and Calorimetry. 119 (2015) 499–506. doi:10.1007/s10973-014-4122-7.

[52] O. Moscoso-Londoño, D. Muraca, L.A.S. De Oliveira, K.R. Pirota, L.M. Socolovsky, The effect of coated- nanoparticles on magnetic properties of ferrogels produced by diffusion route, IEEE TRANSACTIONS ON MAGNETICS. 49 (2013) 4551–4554.

[53] M. Mosiewicki, J. Borrajo, M.I. Aranguren, Mechanical properties of woodflour/linseed oil resin composites, Polymer International. 54 (2005) 829–836. doi:10.1002/pi.1778.

[54] U. Casado, N.E. Marcovich, M.I. Aranguren, M.A. Mosiewicki, High-strength composites based on tung oil polyurethane and wood flour: effect of the filler concentration on the mechanical properties, Polymer Engineering And Science. 49 (2009) 713–721. doi:10.1002/pen.

[55] B. Pukánszky, F. Tüdös, J. Jančař, J. Kolařik, The possible mechanisms of polymer-filler interaction in polypropylene-CaCO3 composites, Journal of Materials Science Letters. 8 (1989) 1040–1042. doi:10.1007/BF01730480.

[56] J.W. Anthony, R.A. Bideaux, W.B. Kenneth, C.N. Monte, Handbook of Mineralogy, Mineralogical Society of America, Chantilly, 2011.

[57] J.R.M. D'Almeida, L.H. De Carvalho, An investigation on the tensile strength of particulate filled polymeric composites, Journal of Materials Science. 33 (1998)

2215–2219. doi:10.1023/A:1004348025804.

[58] M.B. Fernández van Raap, P. Mendoza Zélis, D.F. Coral, T.E. Torres, C. Marquina, G.F. Goya, F.H. Sánchez, Self organization in oleic acid-coated CoFe2O4 colloids : a SAXS study, Journal of Nanoparticle Research. 14 (2012) 1072. doi:10.1007/s11051-012-1072-5.

[59] O. Moscoso-Londoño, P. Tancredi, D. Muraca, P. Mendoza Zélis, D. Coral, M.B. Fernández van Raap, U. Wolff, V. Neu, C. Damm, C.L.P. de Oliveira, K.R. Pirota, M. Knobel, L.M. Socolovsky, Different approaches to analyze the dipolar interaction effects on diluted and concentrated granular superparamagnetic systems, Journal of Magnetism and Magnetic Materials. 428 (2017) 105–118. doi:10.1016/j.jmmm.2016.12.019.

[60] O. Moscoso-londoño, P. Tancredi, D. Muraca, P.M. Zélis, D. Coral, M.B.F. Van Raap, U. Wol, V. Neu, C. Damm, C.L.P. De Oliveira, K.R. Pirota, Di ff erent approaches to analyze the dipolar interaction e ff ects on diluted and concentrated granular superparamagnetic systems, Journal of Magnetism and Magnetic Materials. 428 (2017) 105–118. doi:10.1016/j.jmmm.2016.12.019.

[61] O. Glatter, O. Kratky, Small Angle X-ray Scattering, Academic Press, New York, 1982.

[62] R. Hernández, J. Sacristán, A. Nogales, T.A. Ezquerra, C. Mijangos, Structural organization of iron oxide nanoparticles synthesized inside hybrid polymer gels derived from alginate studied with small-angle X-ray scattering, Langmuir. 25 (2009) 13212–13218. doi:10.1021/la902441s.

[63] G. Beaucage, Approximations leading to a unified exponential/power-law approach to small-angle scattering, Journal of Applied Crystallography. 28 (1995) 717–728.

doi:10.1107/S0021889895005292.

[64] G. Beaucage, H.K. Kammler, S.E. Pratsinis, Particle size distributions from small-angle scattering using global scattering functions research papers, Journal of Applied Crystallography. (2004) 523–535. doi:10.1107/S0021889804008969.

[65] S.-H. Chen, J. Teixeira, Structure and fractal dimension of protein-detergent complexes, Physical Review Letters. 57 (1986) 2583–2586. doi:10.1103/PhysRevLett.57.2583.

[66] L.M. Socolovsky, O. Moscoso Londoño, Complex Magnetic Nanostructures. Consequences of Magnetic Interaction Phenomena in Granular Systems., Springer, Cham, 2017.

[67] P. Allia, M. Coisson, P. Tiberto, F. Vinai, M. Knobel, M. Novak, W. Nunes, Granular Cu-Co alloys as interacting superparamagnets, Physical Review B. 64 (2001) 1–12. doi:10.1103/PhysRevB.64.144420.

[68] M. Knobel, W.C. Nunes, L.M. Socolovsky, E. De Biasi, J.M. Vargas, J.C. Denardin, Superparamagnetism and other magnetic features in granular materials : A review on ideal and real systems, Journal of Nanoscience and Nanotechnology. 8 (2008) 2836–2857. doi:10.1166/jnn.2008.

[69] P.C. Rivas Rojas, P. Tancredi, O.M. Londoño, M. Knobel, L.M. Socolovsky, Tuning dipolar magnetic interactions by controlling individual silica coating of iron oxide nanoparticles, Journal of Magnetism and Magnetic Materials. 451 (2018) 688–696. doi:10.1016/j.jmmm.2017.11.099.

[70] D.H. Han, J.P. Wang, H.L. Luo, Crystallite size effect on saturation magnetization of fine ferrimagnetic particles, Journal of Magnetism and Magnetic Materials. 136 (1994) 176–182.

[71] M.P. Morales, S. Veintemillas-Verdaguer, M.I. Montero, C.J. Serna, A. Roig, L. Casas, B. Martínez, F. Sandiumenge, Surface and internal spin canting in γ-Fe2O3 nanoparticles, Chemistry of Materials. 11 (1999) 3058–3064. doi:10.1021/cm991018f.

[72] C. Meiorin, O.M. Londoño, D. Muraca, L.M. Socolovsky, K.R. Pirota, M.I. Aranguren, M. Knobel, M.A. Mosiewicki, Magnetism and structure of nanocomposites made from magnetite and vegetable oil based polymeric matrices, Materials Chemistry and Physics. 175 (2016) 81–91. doi:10.1016/j.matchemphys.2016.02.071.

[73] J.M. Vargas, W.C. Nunes, L.M. Socolovsky, M. Knobel, D. Zanchet, Effect of dipolar interaction observed in iron-based nanoparticles, Physical Review B - Condensed Matter and Materials Physics. 72 (2005) 2–7. doi:10.1103/PhysRevB.72.184428.

SUPPORTING INFORMATION

STRUCTURAL ANALYSIS OF MAGNETIC NANOCOMPOSITES BASED ON CHITOSAN

Gianina A. Kloster[a], Diego Muraca[b], Oscar Moscoso Londoño[b,c], Marcelo Knobel[b], Norma E. Marcovich[a] and Mirna A. Mosiewicki[a*]

Structural studies of the magnetic particles

Figure S1 shows the X-ray diffraction pattern of the synthesized particles. The positions and relative intensities of the diffraction peaks agree with those of a pure face-centered cubic (fcc) spinel-inverse iron oxide phase corresponding to the standard crystal of magnetite and/or maghemite [28-31]. The crystal size (D) was determined using Scherrer's equation [32-34] (Eq.1), from which a value of D = 9.5 nm was obtained.

$$D = \frac{0.9 * \lambda}{\beta * \cos\theta} \quad (1)$$

where λ is the radiation wavelength (Cu K_α =0.1546 nm), β is the width at half height of the selected peak (in this case (311) plane) and θ is the Bragg angle.

Despite that "crystallite size" is not necessarily synonymous of "particle size", this method gives an estimation of the diameter of the magnetic particles [27]. Notice that the obtained value is close to those determined from TEM images.

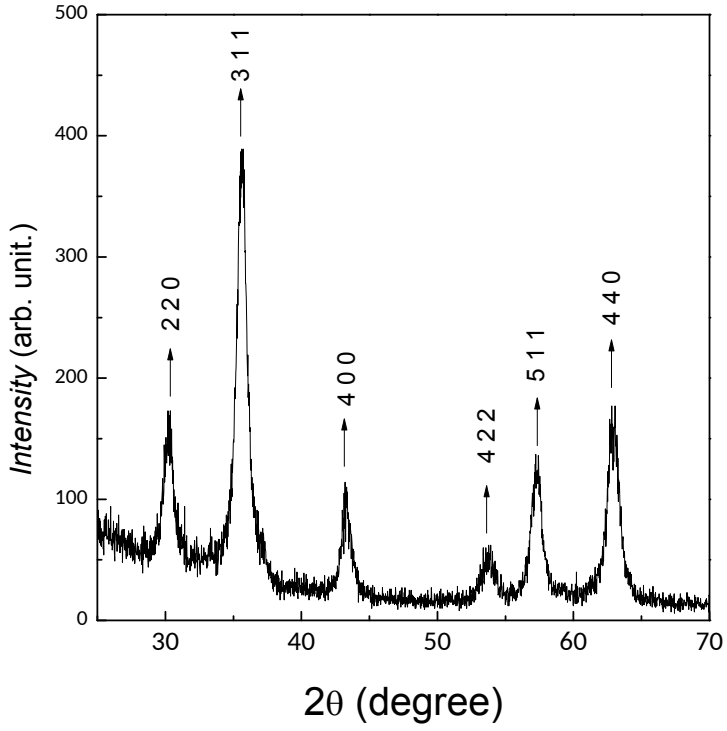

Figure S1. X-ray diffraction pattern of MNPs.

Small-angle X-ray scattering (SAXS) technique was used to analyze the morphological features of magnetite NPs before they are loaded into the chitosan matrices.

Figure S2a presents the SAXS scattering patterns obtained from the synthesized NPs. According to the parameters *q*-range selected for the measurement, the NPs that could be characterized should have sizes ranging between π/q_{max}=1 nm to π/q_{min} = 30 nm. From linear Guinier law at low q region (Figure S2b) the radius of gyration, *Rg*, was calculated as 6 nm, using the following equation [35,36].

$$I(q)=Gexp(-q^2Rg^2/3) \quad (2)$$

Then, if the NPs are mostly spherical, an average diameter, *Dg*, of 15.4 nm was estimated (from $Dg=2(5/3)^{1/2}Rg$), indicating that possibly small aggregation of primary particles occurs when they are in a colloidal suspension during their synthesis. The scattering

intensity in the Porod region presents a slope close to -4, which corresponds to individual particles with smooth surfaces [36,37].

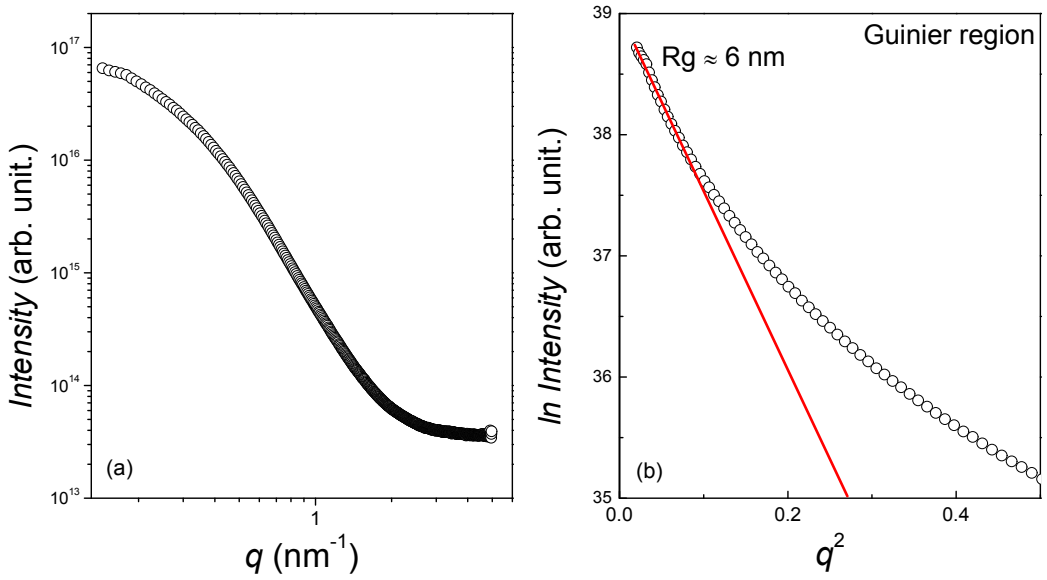

Figure S2. (a) Log–Log curve of small angle X-ray scattering intensity (I) vs. momentum transfer vector (q). (b) Guinier curve (ln I vs q^2). Both for iron oxide NPs.